ISTITUTO NAZIONALE DI FISICA NUCLEARE

**Sezione di Padova**

**INFN/AE-03/05**
**November 3 2003**

# MONTE CARLO SIMULATION OF THE SPS WANF NEUTRINO FLUX

G. Collazuo1[1] and A. Guglielmi

*INFN, Sezione di Padova, Dip. di Fisica "G. Galilei", I-35131 Padova, Italy*

**Abstract**

The method developed for the calculation of the West Area Neutrino Beam used by NOMAD at the CERN SPS for the $\nu_\mu \to \nu_\mu$ and $\nu_\mu \to \nu_e$ oscillation searches is described. The calculation is based on particle production computed using a recent version of FLUKA suitably tuned to SPY and NA20 results on hadron production. The neutrino fluxes were predicted with an uncertainty of about 8% for $\nu_\mu$ and $\nu_e$, 10% for $\bar{\nu}_\mu$, and 12% for $\bar{\nu}_e$. The energy-dependent uncertainty achieved on the $\bar{\nu}_e / \nu_\mu$ ratio ranged from 4 to 7% whereas its normalization uncertainty was 4.2%.

[1]*now at Scuola Normale Superiore di Pisa, Italy.*

PACS.: 14.60.Lm; .29.27.-a; 14.60.Pq

*Published by* ***SIS–Pubblicazioni***
*Laboratori Nazionali di Frascati*

## 1 Introduction

The WANF neutrino beam [1] used by the NOMAD [2] and CHORUS [3] experiments at CERN SPS was produced by the decay of mesons originating in the interaction of 450 GeV/c protons with a beryllium target. The NOMAD experiment was searching for $\nu_\mu \rightarrow \nu_\tau$ [4] and $\nu_\mu \rightarrow \nu_e$ oscillations in a such predominantly $\nu_\mu$ beam, where the $\nu_\tau$ natural contamination was estimated to be at the $\sim 5 \cdot 10^{-6}$ level [5]. The $\nu_\mu \rightarrow \nu_\tau$ search requires the understanding of the major beam component $\nu_\mu$ in order to interpret any potential oscillation signal, and of the minor beam components in order to calculate reliably related backgrounds. Oscillations between $\nu_\mu$ and $\nu_e$ would be evidenced by a distortion of the energy distribution of the $\nu_e$ sample by an excess of the $\nu_e$ events at low energy with respect to the intrinsic beam component. Therefore a precise prediction of $\nu_e/\nu_\mu$ ratio and a sound evaluation of its systematic uncertainty are crucial.

This paper describes the WANF neutrino beam Monte Carlo calculation with a particular emphasis on the secondary particle production in the initial p-Be interaction at 450 GeV/c, one of the most critical items in the simulation. A detailed study of systematic errors on the neutrino beam components and on the predicted $\nu_e/\nu_\mu$ ratio is also presented.

## 2 The WANF neutrino beam Monte Carlo prediction

The general layout of the WANF beam line, is illustrated in Fig. 1. The neutrino beam was produced by 450 GeV/c protons interacting with a special beryllium target. Positive (negative) mesons, mainly $\pi^+$ and $K^+$ produced in one forward direction, were focused (defocused) by two magnetic lenses, horn and reflector, placed downstream of the target, in a $\sim 290$ m long vacuum decay tunnel where neutrinos were produced.

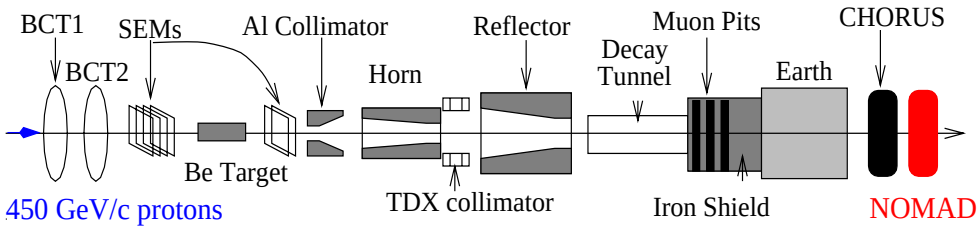


Figure 1: Schematic draw of the WANF beam line at the CERN SPS.

A large iron and earth shield placed at the end of the decay volume filtered out particles other than neutrino upstream of the CHORUS and NOMAD detectors, the latter at 835 m from the Be target.

Neutrinos in the beam originated from the decay of mesons produced through four different mechanisms: proton-Be interactions in the target, proton interactions downstream of the the target in the material other than beryllium, reinteractions of secondaries in the target and downstream of the target and prompt decay of mesons and charmed particles in the target area and beam dump (prompt neutrinos).
The WANF neutrino beam simulation was performed with a new Monte Carlo where the secondary particle production in the Be target by 450 GeV/c proton beam was calculated by a recent release of FLUKA code [6] and which accounts for the measured profiles of the primary proton beam and the detailed structure of the target box. These particle yields were suitably reweighted to take into account the results of NA20 [7] and SPY [8] experiments on meson production.
As a second step the secondaries were propagated down to the NOMAD detector using an especially designed beam-line simulation program, NUBEAM, which includes a detailed description of the focusing system and of the materials of the beam-line [9]. This program, based on GEANT 3.21 package and the 1992 version of FLUKA, GFLUKA, implemented within it, accounted for energy losses, multiple scattering, reinteractions and decays of particles [10]. Particular attention was also devoted to the treatment of meson production by high energy protons escaping the target and hadronic particle reinteractions in the beam-line downstream of the Be target. The meson yields produced in these processes by GFLUKA were properly reweighted for the corresponding ones as obtained with the more recent FLUKA code. The semileptonic $K^{\pm}$ and $K^0_L$ decays were treated in the simulation program according to the V-A structure of the weak leptonic current and the $K_{e3}$ form factor. Pure V-A muon decays were simulated assuming that muons (produced mainly in pion decays) are fully polarized.

In total, $3 \cdot 10^7$ proton interactions were generated by FLUKA and the particles produced were propagated with this Monte Carlo code through the WANF beam-line up to the NOMAD detector. In order to increase the neutrino yield statistics, the decay of each particle with a neutrino among its decay products was repeated 100 times; each time the decay mode was randomly chosen according to its branching ratios and the kinematics of the decay generated anew. A total equivalent statistics of $3 \cdot 10^9$ p.o.t was studied, and the effect of the multiplicity decay factor on statistical errors of the Monte Carlo distribution was also properly taken into account [11].

### 2.1 The primary 450 GeV/c proton beam and the Be target

The primary 450 GeV/c proton beam was extracted from the SPS twice per 14.4 s cycle; each spill, 3 ms long, contained $\sim 1.8 \times 10^{13}$ protons. The beam intensity was measured

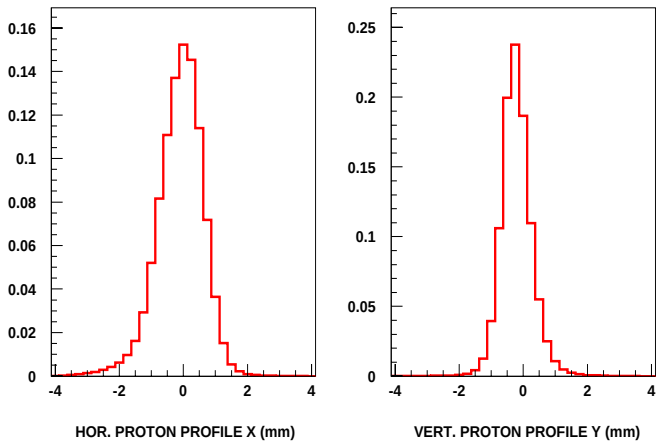


Figure 2: Average horizontal and vertical profiles of the primary proton beam as measured at the entrance of the target box. The proton intensity on the vertical axes is expressed in a.u.

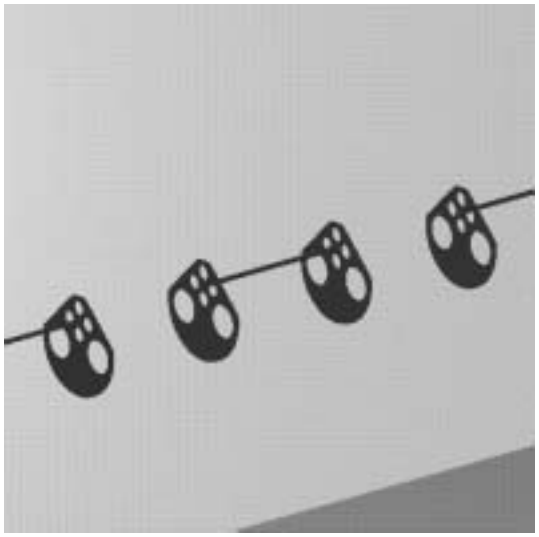

Figure 3: The Be rods structure.

with two beam current transformers (BCTs) and a secondary emission monitor (SEM) placed just upstream of the target. The alignment of the beam with respect to the target was checked by measuring the ratio of pulse heights in two SEM's, one downstream of the target and one upstream. The centering and width of the primary proton beam on target was also measured periodically with a horizontal and a vertical beam scanner each consisting of a wire moved in steps across the beam. The measured proton profiles, averaged over the 2 spills and over all data taking periods, were used as input to the

simulation program (Fig. 2). The corresponding full width at half maximum was 1.7 mm in $X$ and 1.0 mm in $Y$.

The target consisted of 11 beryllium rods, each 3 mm in diameter and 100 mm long, separated by 90 mm. The rods were supported by special Be disks, 2 mm thick, and enclosed in an aluminum target box where they were cooled by gaseous helium flow (Fig. 3). Globally the target amounted to 2.7 nuclear interaction lengths resulting in only $6.7\%$ of the protons not undergoing inelastic interactions in it. The entrance and exit windows of the box consisted of 60 mm diameter titanium foils each 0.1 mm thick. Accounting for the measured proton beam profiles only 5.2 $\%$ of protons missed the target.

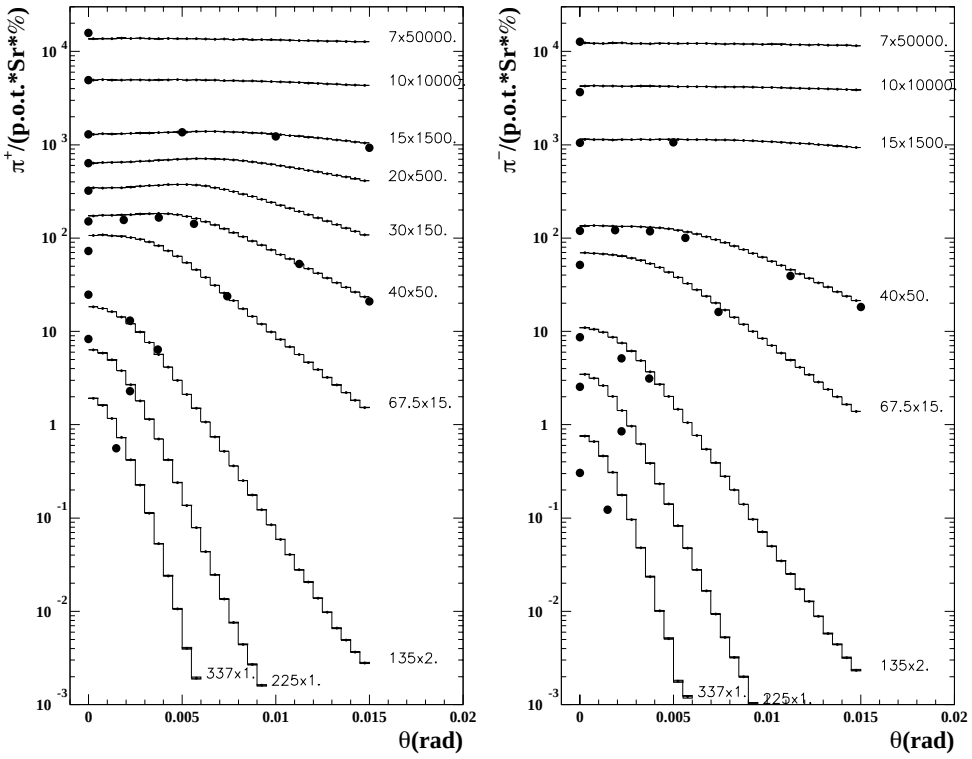


Figure 4: Pion yields from 450 GeV/c protons on 100 mm Be target as a function of the production angle $\theta$ for different $\pi$ momenta as predicted by FLUKA (histograms) and compared with the SPY ($p \leq 40$ GeV/c) and the NA20 data ($p \geq 67.5$ GeV/c), the last properly rescaled for the different primary beam momentum. The first number attached to each histogram is the $\pi^{\pm}$ momentum. The second number is the factor by which both the data and the Monte Carlo prediction were rescaled to be accommodated on the plot.

The target box was surrounded laterally by iron and marble shielding slabs and in the forward direction by a copper and an aluminum collimators which defined an average

angular acceptance of $\sim 10$ mrad for secondaries produced at the target.

### 2.2 High energy proton-Be interactions

One of the most critical element in the prediction of the neutrino fluxes is the description of the yield of particles in proton-target interactions. Direct measurements of $\pi$ and $K$ and $p$ production in Be by protons were performed with this purpose by the NA20 Collaboration at 400 GeV/c [7] and, more recently at 450 GeV/c, by the SPY Collaboration [8] with a precision on the $K/\pi$ ratio of better than $3\%$. These measurements covered complementary ranges of secondary particle momenta, from 60 GeV/c to 300 GeV/c and from 7 GeV/c to 135 GeV/c, respectively.

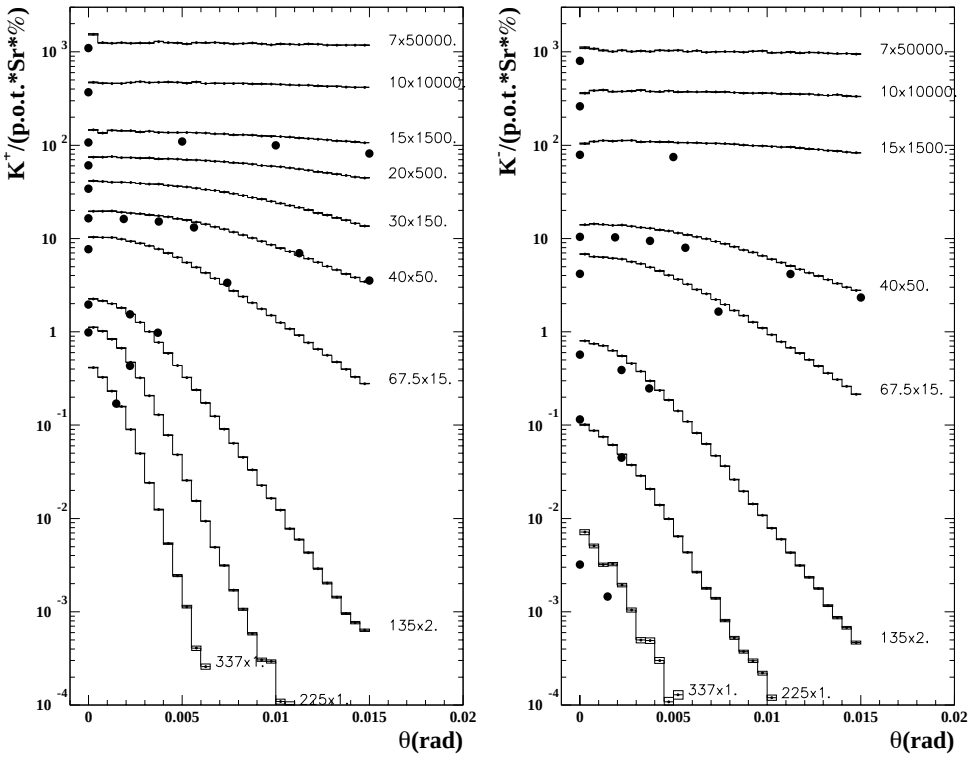


Figure 5: Kaon yields from 450 GeV/c protons on 100 mm Be target as a function of the production angle $\theta$ for different values of $K$ momentum as predicted by FLUKA and compared with the SPY and the NA20 data (see fig. 4 for explanation of the symbols).

The generators of hadronic interactions in the Monte Carlo package generally reproduce with poor accuracy these high energy proton-Be interactions limiting the sensitivity to neutrino oscillation searches. Detailed studies pointed out the FLUKA code as one of

the most suitable hadronic generator for these purposes [12]. FLUKA is a general purpose Monte Carlo package which was successfully tested over a variety of experimental data. It contains, in particular, a detailed description of hadron-nucleon and hadron-nucleus interactions which is based on the Dual Parton Model complemented by the simulation of nuclear reinteractions [13].

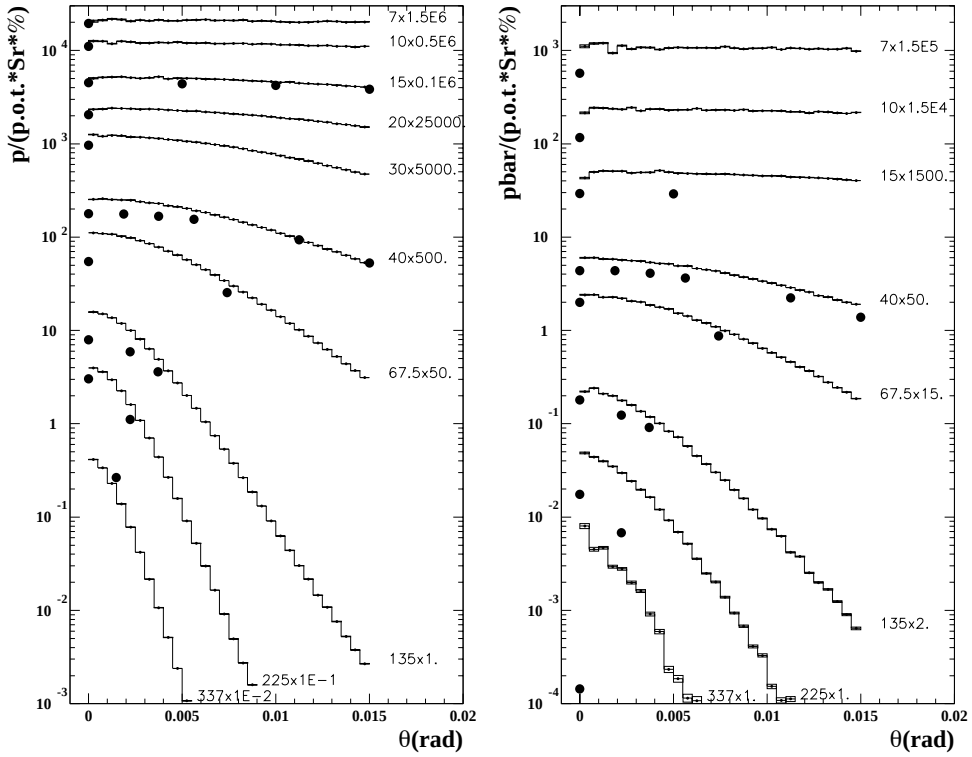


Figure 6: Proton yields from 450 GeV/c protons on 100 mm Be target as a function of the production angle $\theta$ for different values of momentum $p$ as predicted by FLUKA and compared with the SPY and the NA20 data (see fig. 4 for explanation of the symbols).

A recent version of the FLUKA code, was used to simulate the yield of secondary particles from the interaction of 450 GeV/c protons on the 100 mm thick Be target of SPY and NA20 experiments. The comparison of FLUKA simulations with SPY and NA20 data was carried out as a function of the secondary particle momentum $p$ and the production angle $\theta$ with respect to the incoming proton beam direction (Figs. 4, 5, 6). The NA20 measurements were properly rescaled for the different primary proton beam momentum. It was found that the yields of secondary $\pi$ and $K$ agree with the experimental data at the level of $20\%$ or better with only a few exceptions, mostly for negative kaons or at large momenta [12]. A lower accuracy was found for the secondary proton production but

sufficient for these purposes because they contribute only to the antineutrino components via secondary reinteractions in the materials of the beam-line. Globally this agreement was considerably better than that obtained with the generators of hadronic interactions implemented within GEANT, i.e. GFLUKA and GHEISHA [12].

### 2.3 The tuning of the proton-Be interactions

Correction functions to secondary particle production in the WANF Be target by the FLUKA generator, were introduced for $\pi^{\pm}$, $K^{\pm}$, $p$ and $\overline{p}$ based on the observed residual differences between the predicted (FLUKA) and measured (SPY and NA20) particle yields in the 100 mm Be target. At 67.5 and 135 GeV/c measurements were available from both NA20 and SPY: they were found to agree within the quoted errors and therefore the average of the two, weighted according to their errors, was considered.

The amount of the available data is limited especially for meson production at angle $\theta$ different from $0^0$. Therefore, the reweighting coefficients were calculated as a function of particle type and momentum $p$ only, averaging over production angle $\theta$. For a selected $p$, both the experimental and FLUKA secondary yields were convoluted with the corresponding WANF angular acceptance and then integrated over all angles up to $\simeq 10$ mrad. The ratio of these two integrals, $r(p)$, was defined as the weight at a given $p$:

$$r(p) = \frac{(\sum_i y_i \cdot 2\,\pi\,\theta_i \cdot \Delta\theta \cdot \epsilon_i)_{\rm DATA}}{(\sum_j y_j \cdot 2\,\pi\,\theta_j \cdot \Delta\theta \cdot \epsilon_j)_{\rm FLUKA}}, \tag{1}$$

where $y_i$ is the particle yield for a selected angle $\theta_i$, $\Delta\theta = 0.2$ mrad is the angular acceptance of the SPY and NA20 spectrometer and $\epsilon_i$ is the acceptance of the transport for the secondaries which contribute to neutrino flux at NOMAD. This parameter was determined via Monte Carlo from the angular distribution $dN/d\theta_i$ of outcoming secondaries at the Be rods which produced neutrinos in NOMAD:

$$\epsilon_i = \frac{d\,N}{d\theta_i} \cdot \frac{1}{y_i\,\theta_i}. \tag{2}$$

For the momentum values where only the yields in the forward direction were measured, the weights were simply the ratios of the measured to predicted yields at $0^0$. This is justified by the fact that below 40 GeV/c the dependence of the yield on the production angle is weak for $\theta \leq 10$ mrad.

The next step was to fit with polynomial functions these set of weights obtained as described above for each of the charged particles at discrete momenta, in order to have

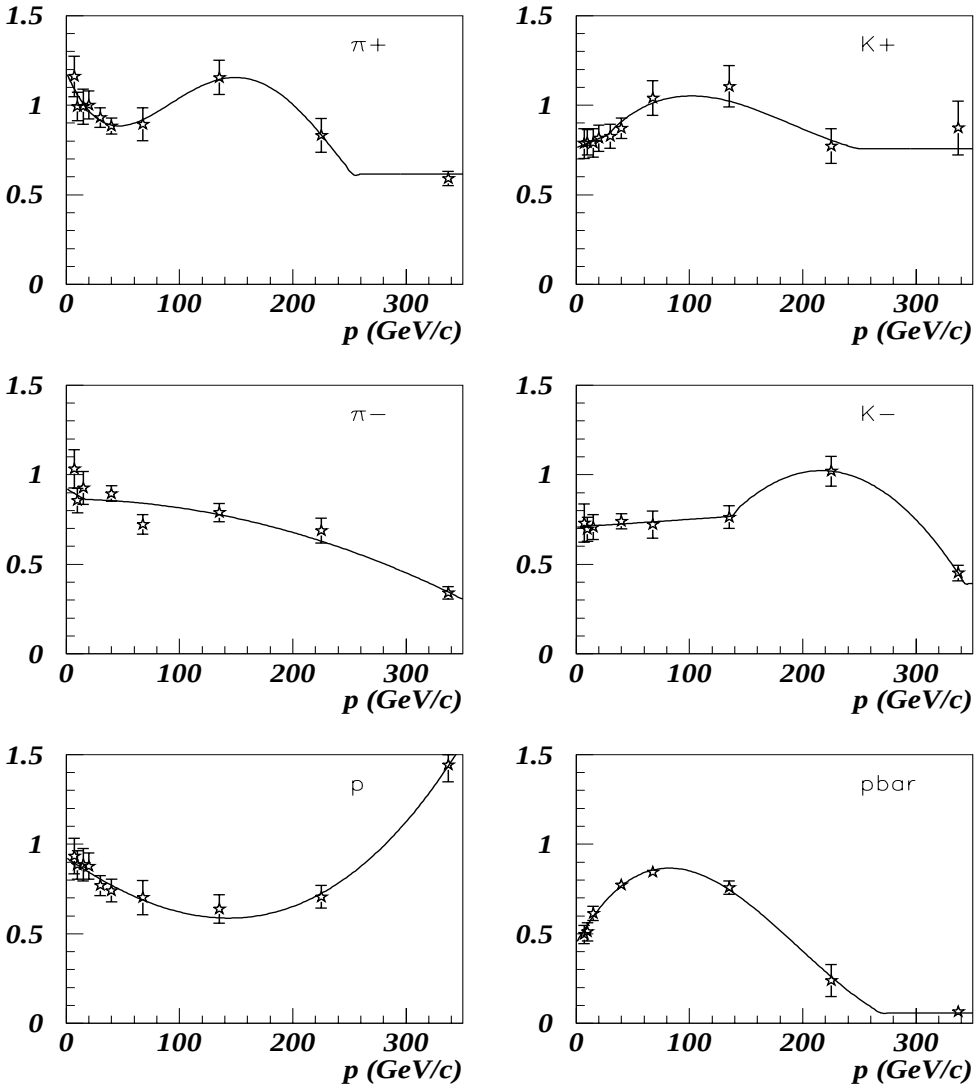


Figure 7: The reweighting function $f$ for $\pi^{\pm}$, $K^{\pm}$, $p$ and $\overline{p}$ obtained from SPY and NA20 measurements. The weights $r(p)$ are shown as a function of the momentum $p$, the curves are the results of fitting them with combination of polynomial functions.

reweighting functions $f$ usable at all momenta (Fig. 7). Systematic and statistical errors of the experimental measurements were combined in quadrature and included in this reweighting procedure and in the fits (see Section 4).

The $K^0_L$ yields were obtained from the SPY and NA20 measurements of $K^+$ and $K^-$ yields using a "quark-counting" model [14]

$$K^0_L = \frac{K^+ + (2n-1)K^-}{2n}, \tag{3}$$

where $n$ is the ratio of u to d structure functions of the proton evaluated at $x_R$, the ratio of the kaon energy in the centre of mass to its maximum possible energy at its $p_T$. This $K^0_L$ parameterization is also well reproduced by FLUKA except for an offset value which depends on the momentum, $a(p)$. Therefore the $K^0$ reweighting function were taken to be a combination of $K^{\pm}$ reweighting functions, $f_{K^{\pm}}(p)$, (Fig. 8):

$$f_{K^0}(p) = (\beta_+(p) f_{K^+}(p) + \beta_-(p) f_{K^-}(p)) \cdot a(p) \tag{4}$$

where the coefficients $\beta_{\pm}(p)$ are determined by $n$ and the $(K^-/K^+)$ yield ratio:

$$\beta_+ = \frac{1}{1 + (2n-1) \cdot (K^-/K^+)} \tag{5}$$

$$\beta_- = \frac{(2n-1) \cdot (K^-/K^+)}{1 + (2n-1) \cdot (K^-/K^+)}. \tag{6}$$

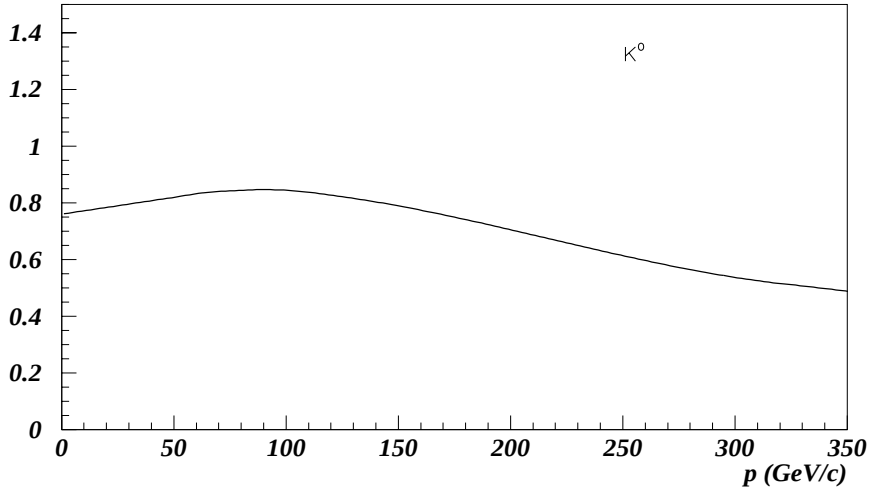


Figure 8: The $K_0$ reweighting function $f_{K_0}$ as a function of momentum $p$.

All the above reweighting functions were then applied on an event-by-event basis to NUBEAM runs, to every $\pi^{\pm}$, $K^{\pm}$, $K^0$, $p$ and $\overline{p}$ emerging from a target rod as a result of the 450 GeV/c primary proton interaction, as a function of the produced particle momentum, and their effects propagated to the neutrino yield in NOMAD detector. Overall $\sim 92\%$ of $\nu_\mu$, $\sim 90\%$ of $\nu_e$, $65\%$ of $\overline{\nu}_\mu$ and $75\%$ of $\overline{\nu}_e$ in NOMAD resulted from this reweighting procedure of the first parent produced in the $p - Be$ interactions.

Neutrinos produced from mesons and charmed particles which decay in the target box or in the beam dump (prompt neutrinos) were treated separately. The remaining neutrinos originated essentially from neutrons produced in the primary $p - Be$ interactions, not affected by the reweighting functions, and by secondary particles generated in the primary protons interactions in the beam line materials downstream of the target.

### 2.4 Prompt neutrinos

The decays of charmed particles produced at the Be target and at the beam-dump as calculated by FLUKA package contributed to neutrinos in NOMAD at the percent level. As a result of a comparison of charm production by $p-Be$ interaction in FLUKA with the existing data, the charmed particle production cross-section was taken to be 0.45 mbarn. The total neutrino contribution from this source, including also the neutrinos from kaons decays in the target box, was small: $0.2\%$ for $\nu_\mu$, $2.7\%$ for $\overline{\nu}_\mu$, $1.7\%$ for $\nu_e$ and $6.7\%$ for $\overline{\nu}_e$.

### 2.5 Interactions of high energy protons and particle reinteractions downstream of the Be target

A fraction of primary protons, which either did not interact in the target or missed it geometrically, interacted in the beam-line elements downstream of the Be target, essentially in the neck of the horn. Their impact on the antineutrino components of the beam was expected particularly large since the mesons of the "wrong" sign (the negative ones) produced in these interactions are not (or only weakly) defocused and have a larger probability of entering the decay tunnel with respect to the negative mesons produced at the Be target. Similarly, the reinteractions of secondary particles in materials downstream of the Be target contributed mainly to the antineutrino component. Therefore, an accurate description of the beam line elements and of the particle yields from these interactions was essential. Both these high energy proton interactions ($p > 440$ GeV/c) and particle reinteractions were simulated in NUBEAM by GFLUKA (as implemented into GEANT3 package) and corrected by the corresponding differences between FLUKA and GFLUKA predictions. In the first case the particle production was corrected by the ratios of the particle yields (Be data as integrated over the WANF acceptance $\sim 10$ mrad) as a function of the particle momentum (Fig. 9). In the second case special simulation runs were performed with both FLUKA and GFLUKA packages in which the material of the beam line was replaced by a 0.5 $\lambda_I$ aluminum slab placed at the position of the neck of the horn. This configuration corresponded to the average amount of material traversed by mesons in the WANF downstream of the Be target at a distance corresponding to the most

likely reinteraction point. The GFLUKA to FLUKA reweighting functions for reinteractions were the ratio of the momenta distributions as determined by the two codes for the different emerging mesons (Fig. 10).
The obtained corrections were applied on an event-by-event basis in the standard NUBEAM runs, as momentum dependent weights to $\pi$'s and $K$'s produced downstream of the Be target by high energy protons and particle reinteraction processes. As a result about $3\%$ of both the $\nu_\mu$'s and the $\nu_e$'s at NOMAD were found to originate from proton interactions downstream of the Be target. The corresponding contribution was, as expected, larger for the antineutrino flux, more than $15\%$ for $\overline{\nu}_\mu$ and about $10\%$ for $\overline{\nu}_e$ flux.

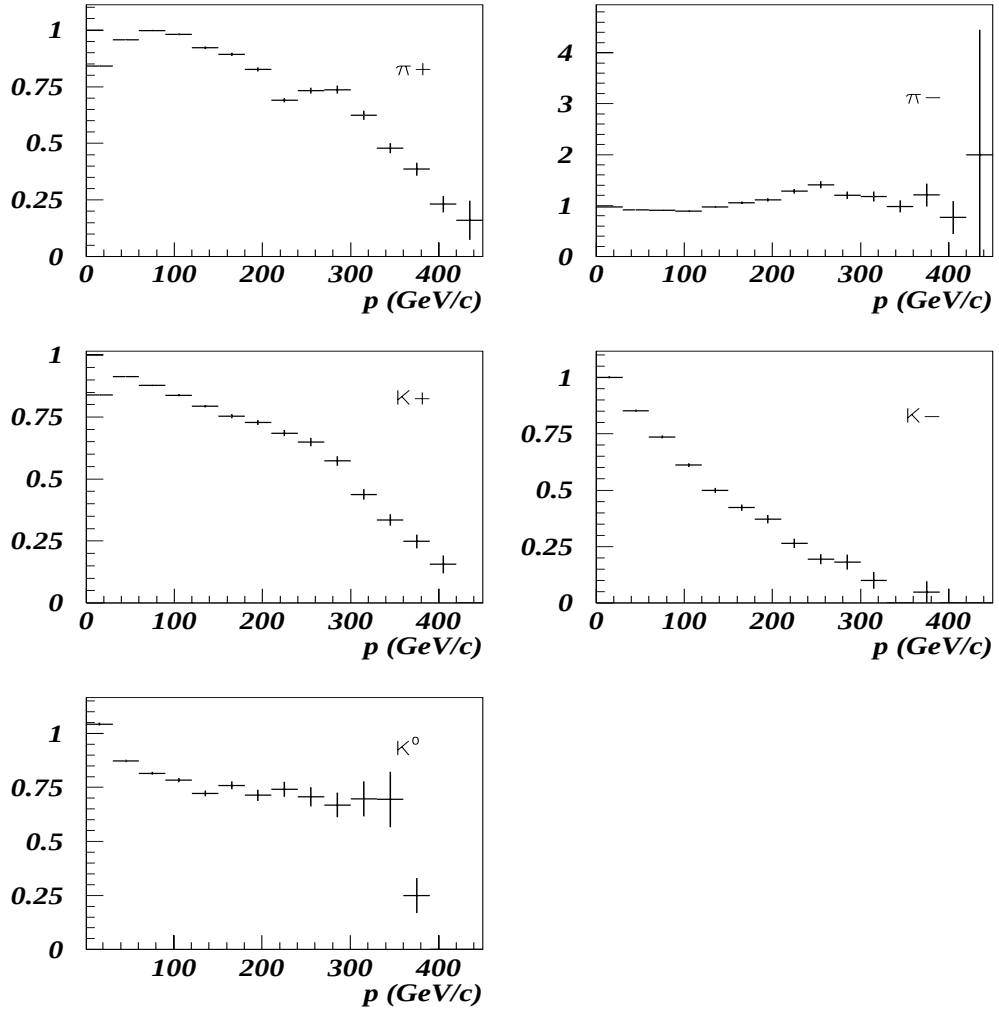


Figure 9: The ratios of FLUKA to GFLUKA high energy proton interaction yield as a function of the momentum $p$.

Similarly, secondary interactions in the materials downstream of the Be target pro-

duced about $10\%$ of $\nu_\mu$'s, $12\%$ of $\nu_e$'s, $\sim$ $45\%$ of $\overline{\nu}_\mu$'s and $24\%$ of $\overline{\nu}_e$'s. The energy spectrum of these neutrinos was significantly softer than the one of neutrinos produced in the decay of mesons which did not experience secondary interactions. The average energies of these two components of the flux were, respectively, 16.7 GeV and 25.2 GeV for $\nu_\mu$ and 19.4 GeV and 39.6 GeV for $\nu_e$. Since a $\nu_\mu \to \nu_e$ oscillation signal would manifest itself as an excess of $\nu_e$ events at low energies, an accurate description of the material downstream of the Be target was crucial to $\nu_\mu \to \nu_e$ oscillation search.

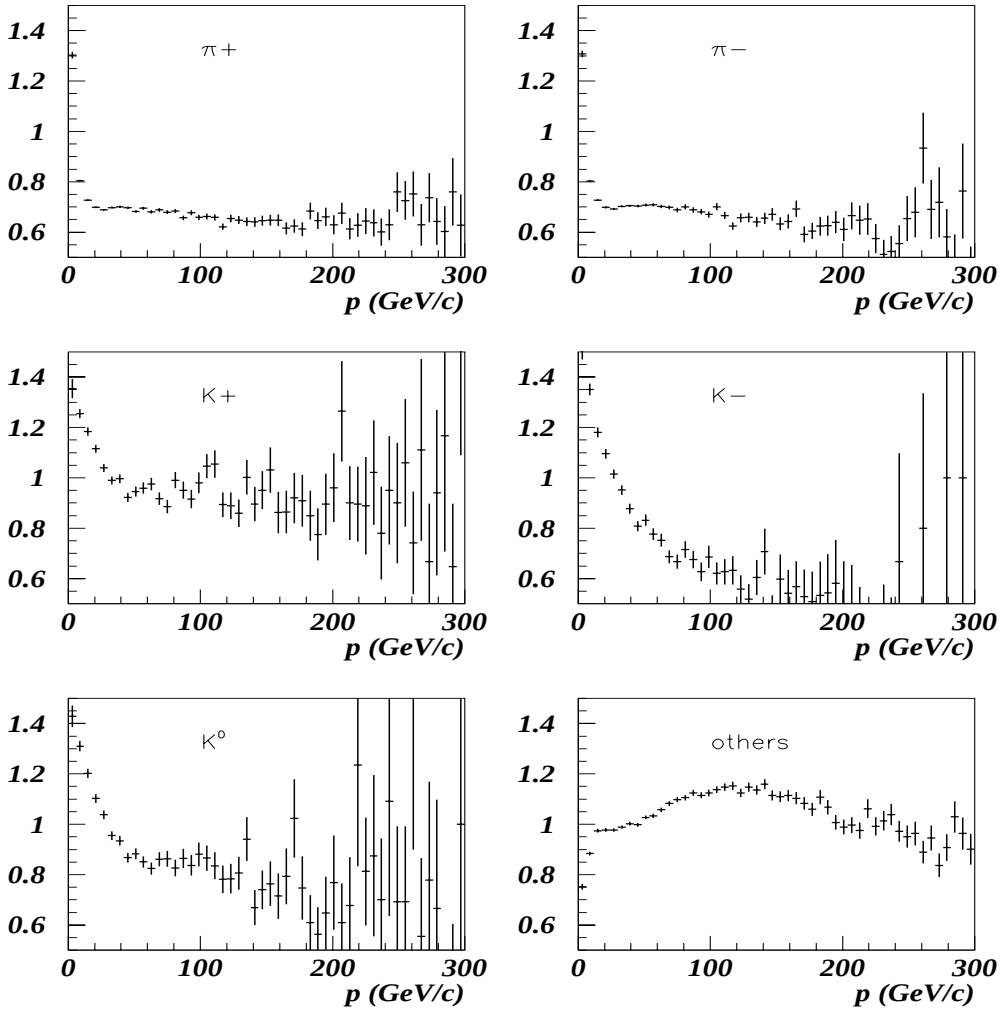


Figure 10: The ratios of FLUKA to GFLUKA particle reinteraction yield as a function of the momentum $p$.

## 3 Neutrino beam flux and composition

According to FLUKA and NUBEAM simulation with the reweight procedures described above, the spectra of the four beam neutrino components $\nu_\mu$, $\overline{\nu}_\mu$, $\nu_e$ and $\overline{\nu}_e$ at the NOMAD detector in a $2.6 \times 2.6$ m$^2$ transversal fiducial area were determined (Fig. 11). The corresponding average energy and relative abundances values and their sources (last parent decay) are reported in Table 1 and 2. It follows that:

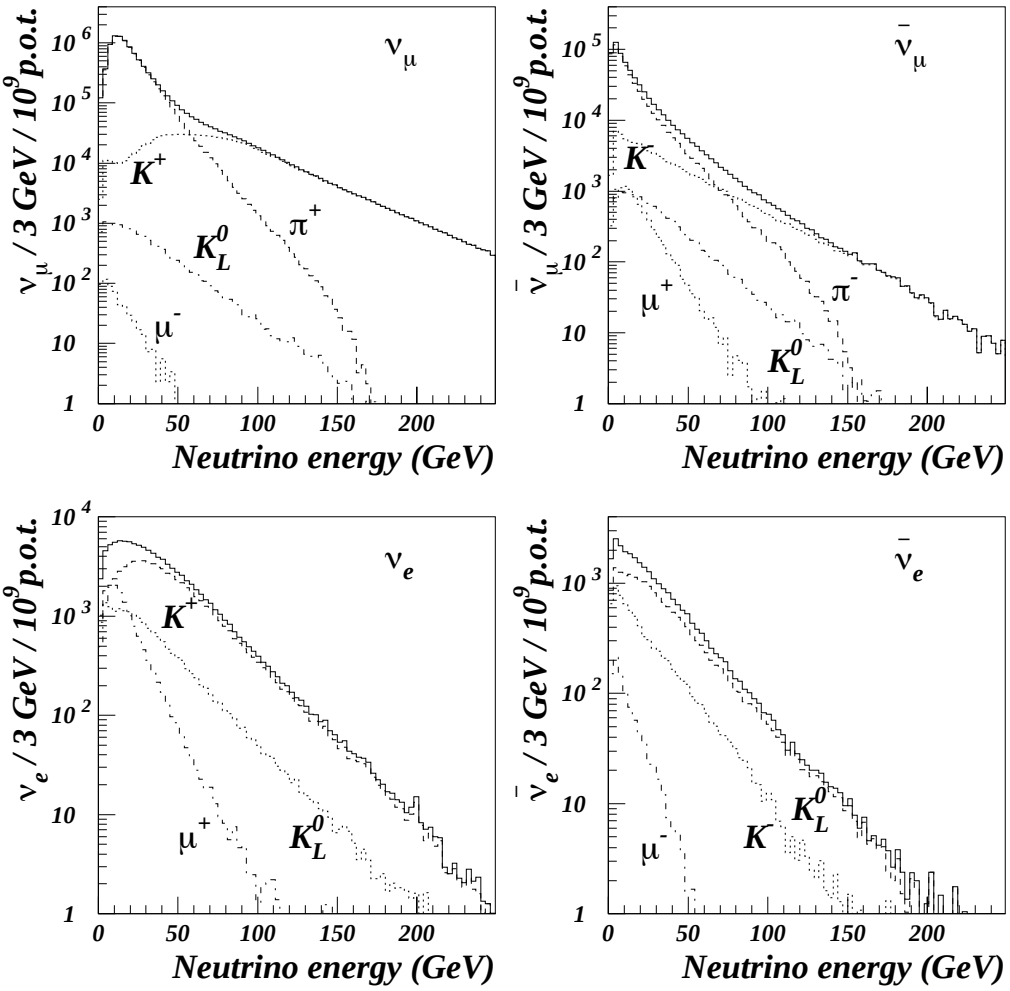


Figure 11: Composition of a) $\nu_\mu$, b) $\overline{\nu}_\mu$, c) $\nu_e$ and d) $\overline{\nu}_e$ spectra at NOMAD within the transverse fiducial area. The single charmed hadron sources, globally at percent level, are not shown.

- The $\nu_\mu$s, $0.94 \times 10^{-2}$ $\nu_\mu/p.o.t$ with an average energy of $24.3$ GeV, are mainly produced via two body decay of $\pi^+$ ($90.4\%$) and $K^+$ ($9.5\%$): neutrinos from $\pi^+$

($K^+$) dominate the $\nu_\mu$ spectrum up to (above) 60 GeV/c.

- Due to the defocusing of the horn and reflector and a lower negative meson cross section production, the $\overline{\nu}_\mu$ fraction is only $\sim 6.8\%$ with an average energy of $\sim 17.2$ GeV. Similarly to $\nu_\mu$ production, $\overline{\nu}_\mu$s are produced via $\pi^-$ and $K^-$ decays. An appreciable fraction is produced by $K^0_L$ and charmed hadrons which are not affected by the defocusing and $\mu^+$ decays (from $\pi^+$).

- The intrinsic $\nu_e$ component is expected to be about $1.0\%$ of the total neutrino beam flux, the average energy is $36.4$ GeV. However this contamination is reduced to $0.5\%$ below 20 GeV. The $\nu_e$ to $\nu_\mu$ ratio as a function of the neutrino energy is shown in Fig. 12. The main contributions are from $K^+_{e3}$ ($68.0\%$) and $K^0_{e3}$ ($17.8\%$) decays, followed by muon ($13.6\%$) and charmed and hyperon ($0.6\%$) decays.

- The principal source of the $\overline{\nu}_e$, less than $0.3\%$ of the neutrino flux, is the $K^0_{e3}$ ($68.2\%$) followed by $K^-_{e3}$ ($25.1\%$), charmed hadron ($3.2\%$) and muon ($3.5\%$) decays.

| Neutrino | intensity $[\nu/p.o.t]$ | $< E_\nu >$ [GeV] | relative ab. |
|---|---|---|---|
| $\nu_\mu$ | 0.94 $\times 10^{-2}$ | 24.3 | 1.0 |
| $\overline{\nu}_\mu$ | | 17.2 | 0.0678 |
| $\nu_e$ | | 36.4 | 0.0102 |
| $\overline{\nu}_e$ | | 27.6 | 0.0027 |

Table 1: Predicted intensity, mean energy and relative abundances for neutrino fluxes (1-300 GeV neutrino energy range) within the $2.6 \times 2.6$ m$^2$ NOMAD transverse fiducial area.

| Neutrino | $\pi^+$ | $\pi^-$ | $K^+$ | $K^-$ | $K^0_L$ | $\mu^+$ | $\mu^-$ |
|---|---|---|---|---|---|---|---|
| $\nu_\mu$ | 90.4 | - | 9.5 | - | 0.1 | - | $< 0.1$ |
| $\overline{\nu}_\mu$ | - | 84.0 | - | 12.8 | 1.9 | 1.2 | - |
| $\nu_e$ | - | - | 68 | - | 17.8 | 13.6 | - |
| $\overline{\nu}_e$ | - | - | - | 25.1 | 68.2 | - | 3.5 |

Table 2: Origin of the four neutrino species (last parent decay).

It was evaluated by previous studies that the use of GFLUKA instead FLUKA as hadronic generator overestimates the neutrino flux by $\sim 15\%$ [12]. The tuning of

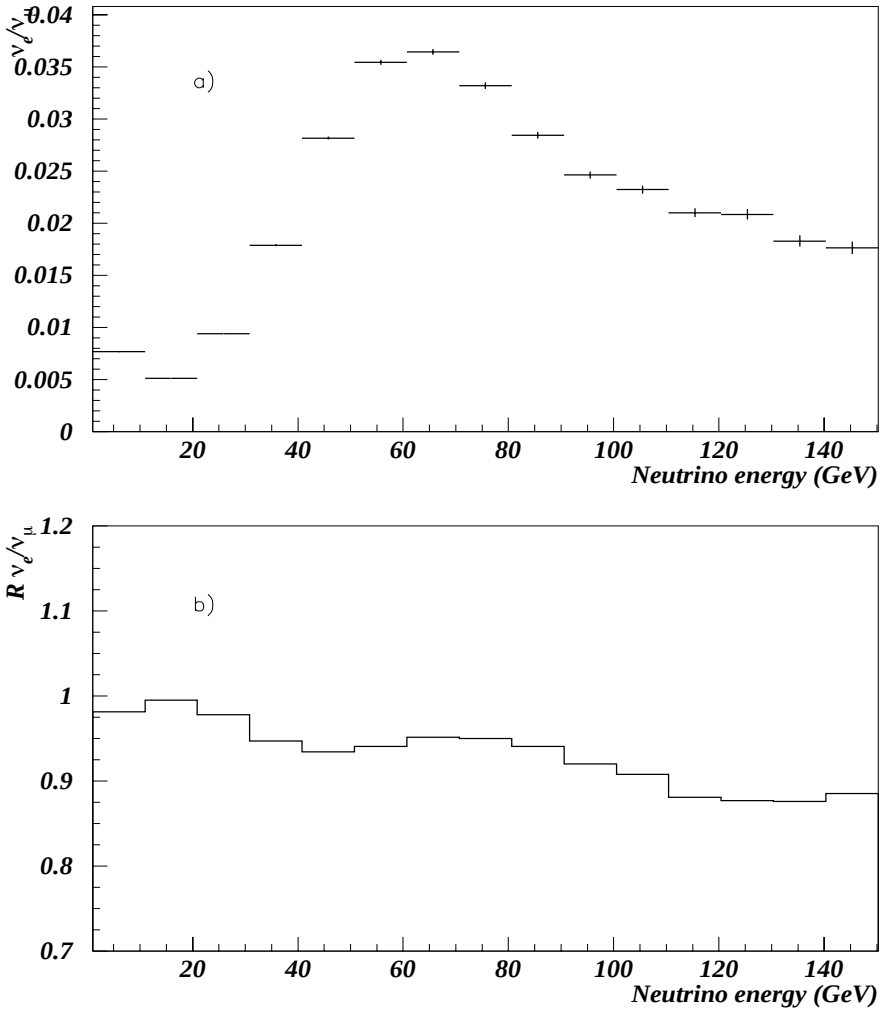


Figure 12: a) The $\nu_e/\nu_\mu$ neutrino flux ratio as a function of neutrino energy; b) the ratio of the $\nu_e/\nu_\mu$ prediction with Be reweighting functions to the corresponding without these reweighting functions.

FLUKA to SPY/NA20 data further reduces the neutrino yield by $\sim 4\%$ and introduces large energy-dependent variations especially on $\overline{\nu}_\mu$. The prediction of $\nu_e/\nu_\mu$ energy dependence (Fig. 12a) is also modified by up to $\sim 10\%$ (Fig. 12b).

## 4 Systematic uncertainties evaluation of the neutrino beam

All the systematic uncertainties connected to the neutrino production processes, namely the $p$-Be interactions in the target, proton interactions downstream of the the target, reinteractions of secondaries in the target and long the beam-line and prompt decay of mesons and charmed particles in the target area and beam dump, were studied and are described in the following Sections. Additional sources of systematics, such as those arising from the position of the beam relative to the target and from the propagation of secondary mesons through the WANF beam line (horn and reflector position and currents, materials, etc.) are also presented.

### 4.1 Systematics from p-Be secondaries production and prompt neutrinos

The major contribution to the systematic uncertainties of neutrino flux prediction is expected from the secondary particle production in Be rods which generated, by direct decay of the mesons produced or by their successive reinteractions and decays, more than $95\%$ of the total neutrino flux in NOMAD.
Regarding to the $\pi^\pm$, $K^\pm$ and $p$ production from 450 GeV/c protons on Be target, two error sources affected the adopted reweighting procedure:

- the statistical and systematic uncertainties of NA20 and SPY measurements, $\Delta_{1,stat}$ and $\Delta_{1,syst}$;
- the systematic uncertainty arising from the use of a single angle-independent correction $r(p)$ for each momentum and particle type, $\Delta_2$.

Both these uncertainties were momentum and particle type dependent.
The first step in the error calculation was to identify the systematic uncertainty $\Delta_{1,syst}$ of SPY and NA20 data directly affecting this analysis, that did not cancel in the $\nu_e/\nu_\mu$ ratio, namely those due to particle selection efficiency and identification, particle dependent losses along the spectrometer, particle decays and stability of the intensity of the primary proton beam and of its position relative to the target. Globally $1.8\%$ of error, mainly due to the absolute p.o.t calibration and to the primary proton profile, was removed in quadrature from the full relative errors quoted in the SPY and NA20 experiments (see Table 3, 4).

| | $P$: GeV/c | 7 | 10 | 15 | 20 | 30 | 40 | 67.5 | 135 | 225 |
|---|---|---|---|---|---|---|---|---|---|---|
| $(\Delta_1)_{stat}$ | | 0.010 | 0.010 | 0.003 | 0.003 | 0.005 | 0.003 | 0.004 | 0.004 | 0.005 |
| $(\Delta_1)_{syst}$ | | 0.096 | 0.079 | 0.098 | 0.078 | 0.057 | 0.046 | 0.051 | 0.062 | 0.065 |
| $\Delta_2$ | | 0.007 | 0.007 | 0.004 | 0.007 | 0.014 | 0.020 | 0.089 | 0.056 | 0.091 |

Table 3: Statistical and systematic relative errors on $\pi^+$ yields.

| | $P$: GeV/c | 7 | 10 | 15 | 20 | 30 | 40 | 67.5 | 135 | 225 |
|---|---|---|---|---|---|---|---|---|---|---|
| $(\Delta_1)_{stat}$ | | 0.045 | 0.025 | 0.028 | 0.019 | 0.014 | 0.009 | 0.010 | 0.010 | 0.005 |
| $(\Delta_1)_{syst}$ | | 0.089 | 0.079 | 0.095 | 0.080 | 0.058 | 0.049 | 0.059 | 0.066 | 0.065 |
| $\Delta_2$ | | 0.035 | 0.035 | 0.013 | 0.035 | 0.055 | 0.042 | 0.071 | 0.080 | 0.107 |

Table 4: Statistical and systematic errors on $K^+$ yields.

The uncertainty $\Delta_2$ arising from the r(p) procedure, was estimated as follows. For momenta where angular scans were available, the uncertainty $\Delta_2$ was estimated as the root mean square deviation between the individual angular measurements $y_i$ available at that momentum $p$ and the corresponding FLUKA values rescaled by the reweighting ratio $r(p)$ as calculated below:

$$\Delta_2^2 = \sum_i^n (y_i^{DATA} - y_i^{FLUKA} \cdot r)^2 \cdot \frac{\theta_i \cdot \epsilon_i}{\sum_j^n \theta_j \cdot \epsilon_j}. \quad (7)$$

For momenta where only the $0^0$ angle was measured, $\Delta_2$ was taken to be the difference between the $0^0$ point and the single-valued reweighting at the angular scan nearest in momentum. Finally all these errors were combined in quadrature to obtain the global resulting error $\Delta$ relative to each $r(p)$ single-value for each particle type (see table 5):

$$\Delta = \sqrt{\Delta_{1,stat}^2 + \Delta_{1,syst}^2 + \Delta_2^2}. \quad (8)$$

The systematic uncertainty on the neutrino flux predictions at NOMAD arising from $\Delta$ and from the use of a fit procedure to interpolate between the discrete experimental measurements of SPY and NA20 was then evaluated as follows. First the following quantities were calculated:

| | $P$: GeV/c | 7 | 10 | 15 | 20 | 30 | 40 | 67.5 | 135 | 225 |
|---|---|---|---|---|---|---|---|---|---|---|
| $\pi^+$ | | 0.097 | 0.080 | 0.098 | 0.078 | 0.059 | 0.050 | 0.103 | 0.084 | 0.112 |
| $K^+$ | | 0.106 | 0.090 | 0.100 | 0.089 | 0.081 | 0.065 | 0.093 | 0.104 | 0.125 |
| $p$ | | 0.106 | 0.090 | 0.103 | 0.084 | 0.073 | 0.084 | 0.137 | 0.124 | 0.090 |
| $\pi^-$ | | 0.103 | 0.079 | 0.099 | | | 0.048 | 0.075 | 0.065 | 0.100 |
| $K^-$ | | 0.146 | 0.096 | 0.098 | | | 0.058 | 0.105 | 0.083 | 0.081 |

Table 5: The $\Delta$ global errors as a function of $p$ for $\pi^{\pm}$, $K^{\pm}$ and $p$.

- the distributions of neutrino fluxes at NOMAD $\phi_\nu$ ($\nu = \nu_\mu, \overline{\nu}_\mu, \nu_e, \overline{\nu}_e$) were generated using NUBEAM and the value of the reweighting functions obtained using the fit as described in the Section $2.3$;

- for each neutrino reaching NOMAD the two-dimensional distribution $M_{par,\nu}(p,\ E)$ was filled as a function of its parent momentum $p$ at the Be rod and of its energy $E$ according to the neutrino and parent type ($par = \pi^{\pm},\ K^{\pm},\ K^0,\ p$);

- the component of the $\nu$ fluxes in NOMAD, $\phi^0_\nu$, not affected by the reweighting (remaining first parents at the Be rod, prompt neutrinos and p-Be interactions downstream of the target) which error was separately evaluated, were determined.

Then three thousand "simulated experiments" were performed; each such experiment consisted of the following steps:

- the discrete measurement of the $r(p)$ yield ratios were modified at random about their central value according to Gaussians with $\Delta$ errors as standard deviations and the fits repeated. This resulted in a new prediction for $\pi^{\pm}$, $K^{\pm}$, and $p$ according to the new set of reweighting functions $f^{trial}(p)$. In this procedure the normalization of the $K^+$ and $K^-$ fits were further modified at random according to a Gaussian of $1.2\%$ width to take into account the uncertainty in $K_{e3}$ branching ratio. The $K^0$ predictions were recalculated by using the new $K^+$ and $K^-$ prediction into the quark-counting formula together with an additional uncertainty generated at random according to a Gaussian with a standard deviation of $15\%$ (the accuracy of the formula);

- the variations $f^{trial}/f$ relative to $\pi^{\pm}$, $K^{\pm}$, $K_0$ and $p$ were propagated to the neutrino flux via the corresponding $M_{par,\nu}(p,\ E)$ distributions; a new energy dependent flux

prediction at NOMAD was obtained for each neutrino species by integrating the modified distributions $M$ over the parent momentum and type

$$\phi_\nu^{trial}(E) = \sum_{par} \sum_{p} M_{par,\nu}(p,\ E) \cdot (\frac{f^{trial}(p)}{f(p)})_{par} + \phi_\nu^0(E) \tag{9}$$

where $\phi_\nu^0$ is the unperturbed neutrino flux;

- in order to separate the uncertainty into an energy dependent uncertainty and an overall normalization uncertainty, the new integral flux of each neutrino species was compared to the integral flux obtained with the central fits $f(p)$:

$$N_\nu = \frac{\sum_E \phi_\nu^{trial}(E)}{\sum_E \phi_\nu(E)}; \tag{10}$$

- these $N_\nu$ ratios were used to renormalize the energy dependent fluxes of the simulated experiment to that of the central value:

$$\phi_\nu^{trial,norm}(E) = \phi_\nu^{trial}(E) \cdot N_\nu \tag{11}$$

and to extract, by comparing these quantities to the corresponding central values, the energy dependent prediction associated to this trial:

$$s_\nu(E) = \frac{\phi_\nu^{trial,norm}(E)}{\phi_\nu(E) + \phi_\nu^0(E)} \tag{12}$$

which was evaluated at $E = 10$, 20, 30,... GeV neutrino energy.

The energy dependent prediction of the $\nu_e/\nu_\mu$ ratio was also obtained for the simulated experiment, as well as the corresponding normalization factor for the $\nu_e$ to $\nu_\mu$ ratio, $N_{e,\mu}$. In Fig. 13, are shown some relevant plots for a $\pi^+$ reweighting variation and the corresponding one for the $\nu_\mu$ flux.
Repeating this procedure for 3000 trials resulted in an envelope of predictions for each neutrino species and for the $\nu_e/\nu_\mu$ ratio from which the energy dependent systematic uncertainty at $68\%$ C.L., $\Delta_\nu$, was extracted. At any neutrino energy it was taken as the

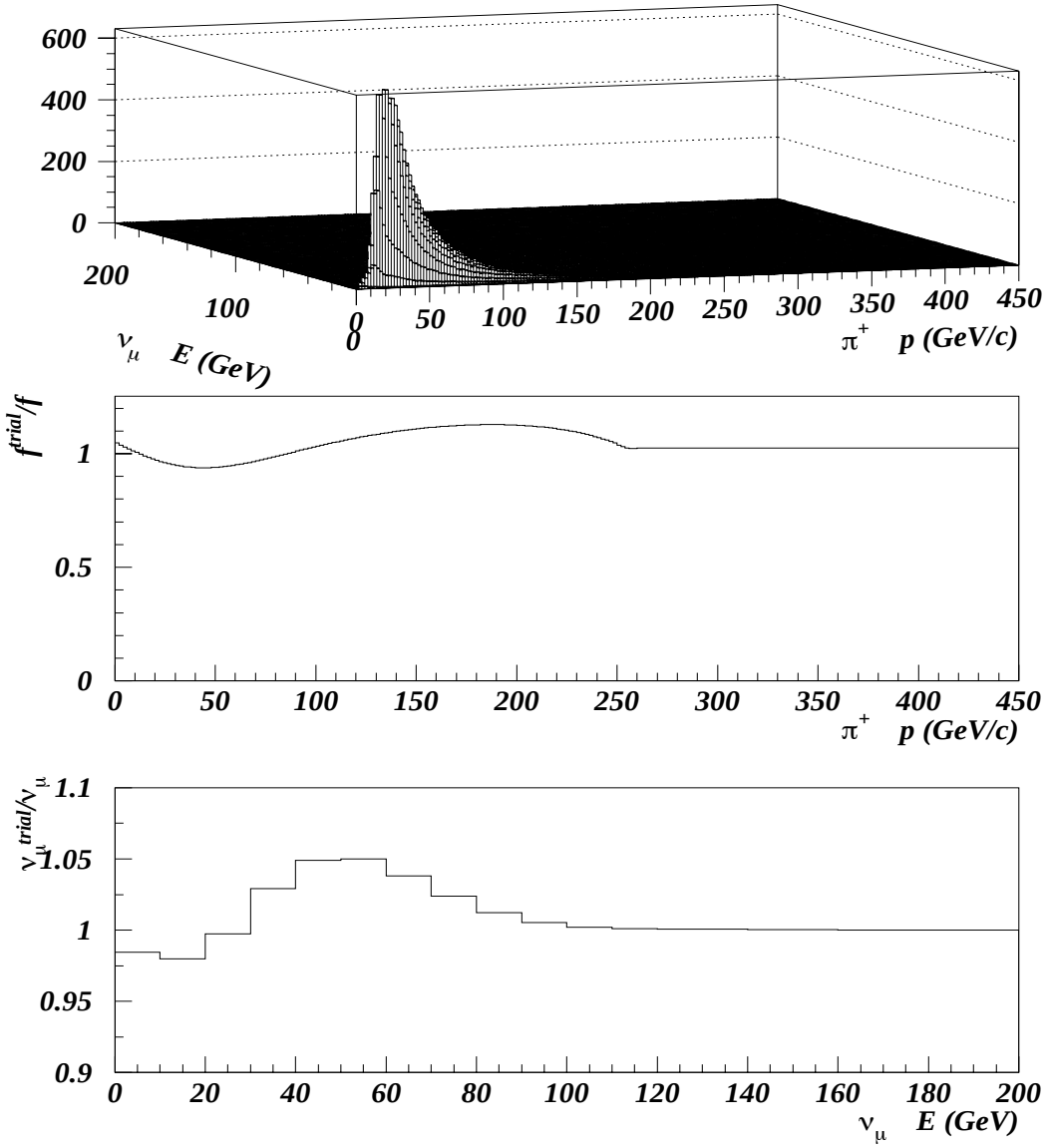


Figure 13: The $\nu_\mu - \pi^+$ correlation histogram $M$ (top), the $f^{trial}/f$ ratio for the $\pi^+$ rew. function (center) and the resulting $\nu_\mu$ spectrum variation (bottom).

r.m.s. with of the envelop at that energy. In Fig. 14 are reported the plots of error band $\Delta_\nu$ as a function of the neutrino energy for $\nu_\mu$, $\overline{\nu}_\mu$, $\nu_e$, $\overline{\nu}_e$ and $\nu_e/\nu_\mu$.
The normalization uncertainty for each neutrino species and for $\nu_e/\nu_\mu$ ratio was determined as the standard deviation of the distribution of the 3000 values of the corresponding integral flux ratio $N_\nu$ (Fig. 15 and Tab. 6). Their standard deviations are 0.029 for $\nu_\mu$, 0.017 for $\overline{\nu}_\mu$, 0.035 for $\nu_e$, 0.060 for $\overline{\nu}_e$ and 0.036 for $\nu_e/\nu_\mu$. Due to correlations between the origins of $\nu_\mu$ and $\nu_e$ fluxes, the uncertainties on the $\nu_e/\nu_\mu$ ratio is smaller than the uncertainties on the individual $\nu_\mu$ and $\nu_e$ fluxes. The standard deviation is smaller for $\overline{\nu}_\mu$ than $\nu_\mu$ because this uncertainty only refers to $\nu_\mu$ and $\overline{\nu}_\mu$ originating from meson produced in the p-Be interactions in the target and, as explained previously, the fraction of $\overline{\nu}_\mu$ at NOMAD from this source is smaller than the corresponding one from $\nu_\mu$.

The systematic uncertainty arising from the yields of the remaining particles produced at a Be rod other than pions, kaons and protons, essentially neutrons muons and antiprotons (referred to as "others") which contributed marginally to neutrino flux, was also subdivided into a normalization and a energy-dependent component. The first error was evaluated by increasing their contributions to neutrino spectra by $10\%$ (see the next Section) resulting in a contribution to the total error of $0.4\%$, $1.5\%$, $0.9\%$ and $0.1\%$ for $\nu_\mu$ $\overline{\nu}_\mu$ $\nu_e$, $\overline{\nu}_e$ and $\nu_e/\nu_\mu$ ratio. The corresponding energy dependent error (Fig. 16) were accounted for by increasing the "others" contribution by $11.2\%$ (see the next Section).

Concerning the prompt neutrinos produced essentially by charmed particles and kaons which decay in the target box and at the dump, a conservative uncertainty of $50\%$ and $20\%$ was assumed for the charm and kaons production respectively, resulting in an energy dependent almost negligible error for $\nu_\mu$ and $\nu_e$ and $\nu_e/\nu_\mu$ ratio. (fig. 17).

### 4.2 Systematics from 450 GeV/c protons interactions and particle reinteractions downstream of the target

Both high energy protons interactions and secondary particle reinteractions in the beamline materials downstream of the Be target were simulated by GFLUKA and the estimates then corrected by the ratio between FLUKA and GFLUKA predictions. The secondaries reinteractions in the target area were directly treated with the FLUKA code. The yields of mesons from these three sources could not be corrected by the reweighting factors $f$ obtained from SPY and NA20 measurements since these experiments did not measure proton interactions in materials other than beryllium nor interactions of particles other than protons. However the determined reweighting factors $f$ for FLUKA to SPY and NA20 data can be used to estimate the uncertainty on the neutrino fluxes from these three sources. For each produced meson type, the two quantities $D_{max}$, the maximum

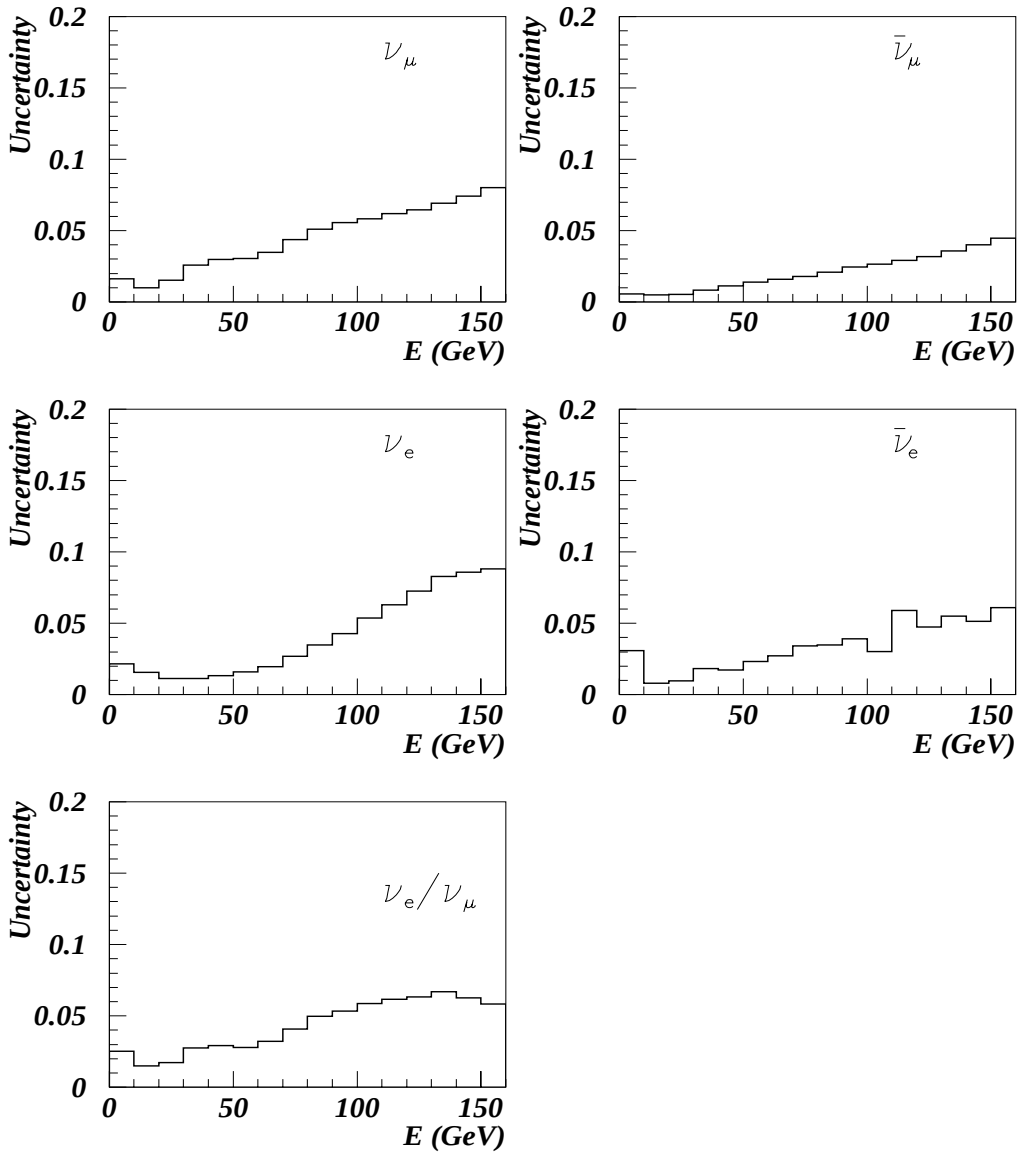


Figure 14: Energy dependent errors on neutrino fluxes and $\nu_e/\nu_\mu$ ratio from $\pi^\pm$, $K^\pm$, $K^0$ and $p$ in the Be target.

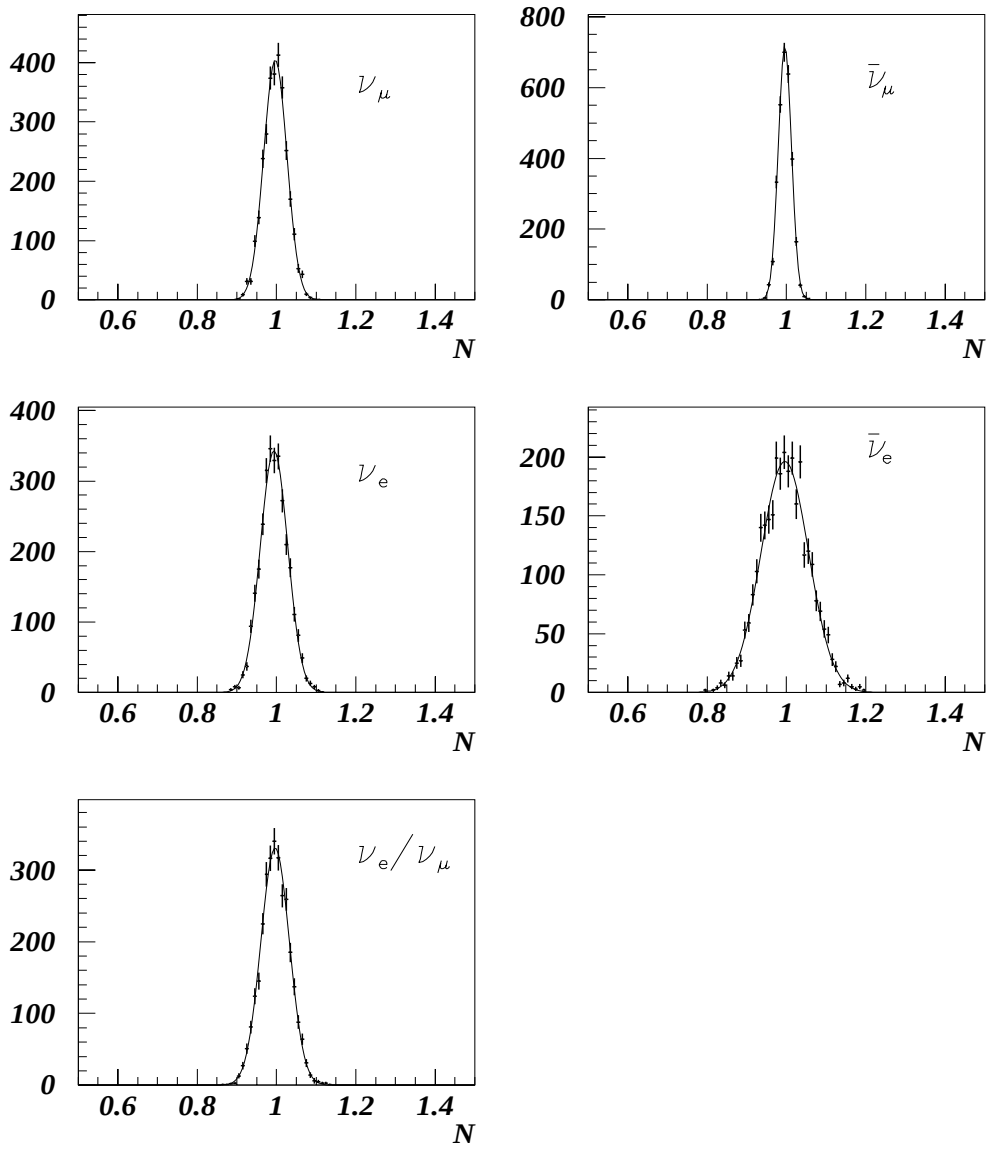


Figure 15: Normalization errors on neutrino fluxes and $\nu_e/\nu_\mu$ ratio from $\pi^\pm$, $K^\pm$, $K^0$ and $p$ production in the Be target.

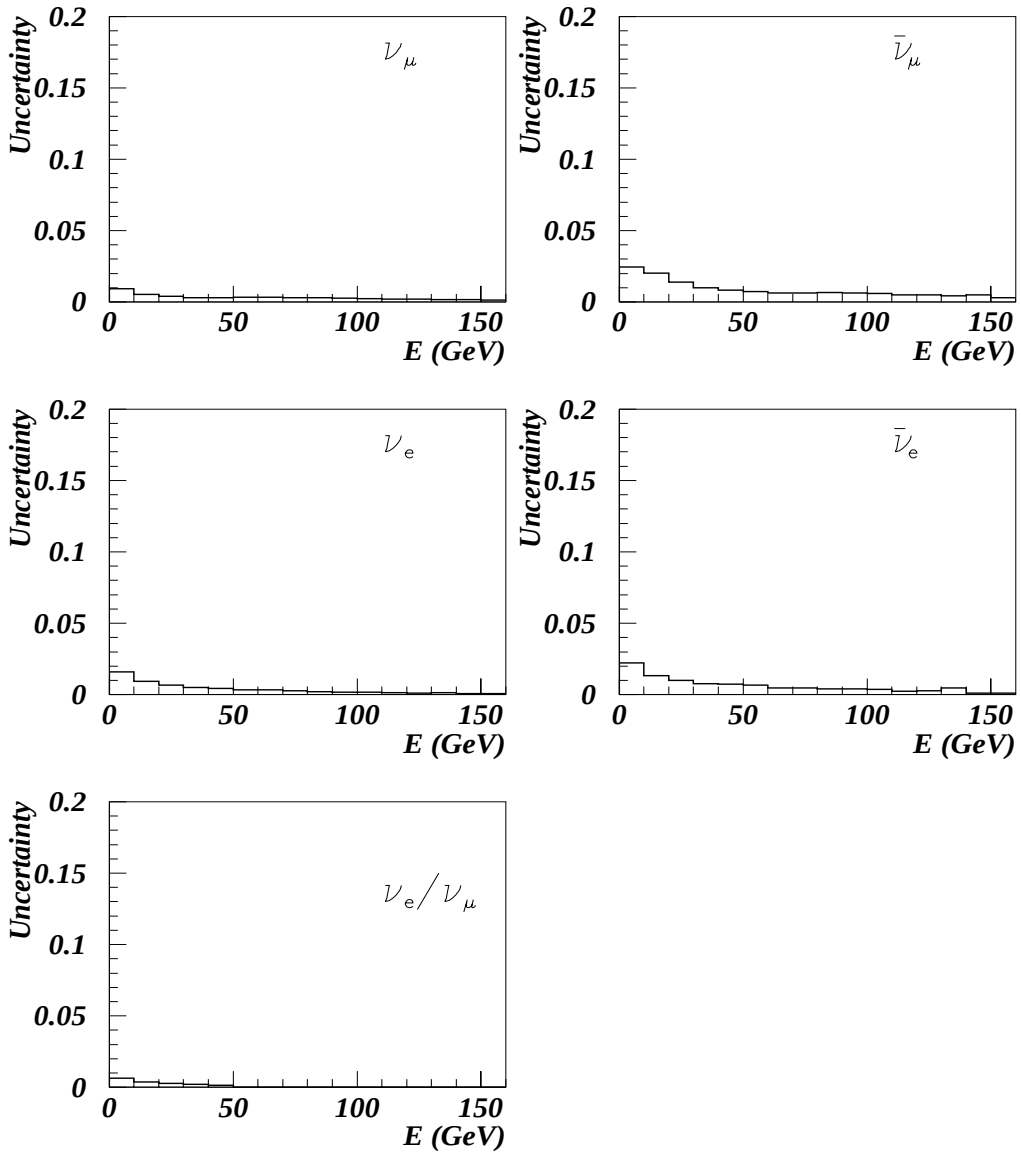


Figure 16: Energy dependent errors on neutrino fluxes and $\nu_e/\nu_\mu$ ratio from "others" production in the Be target.

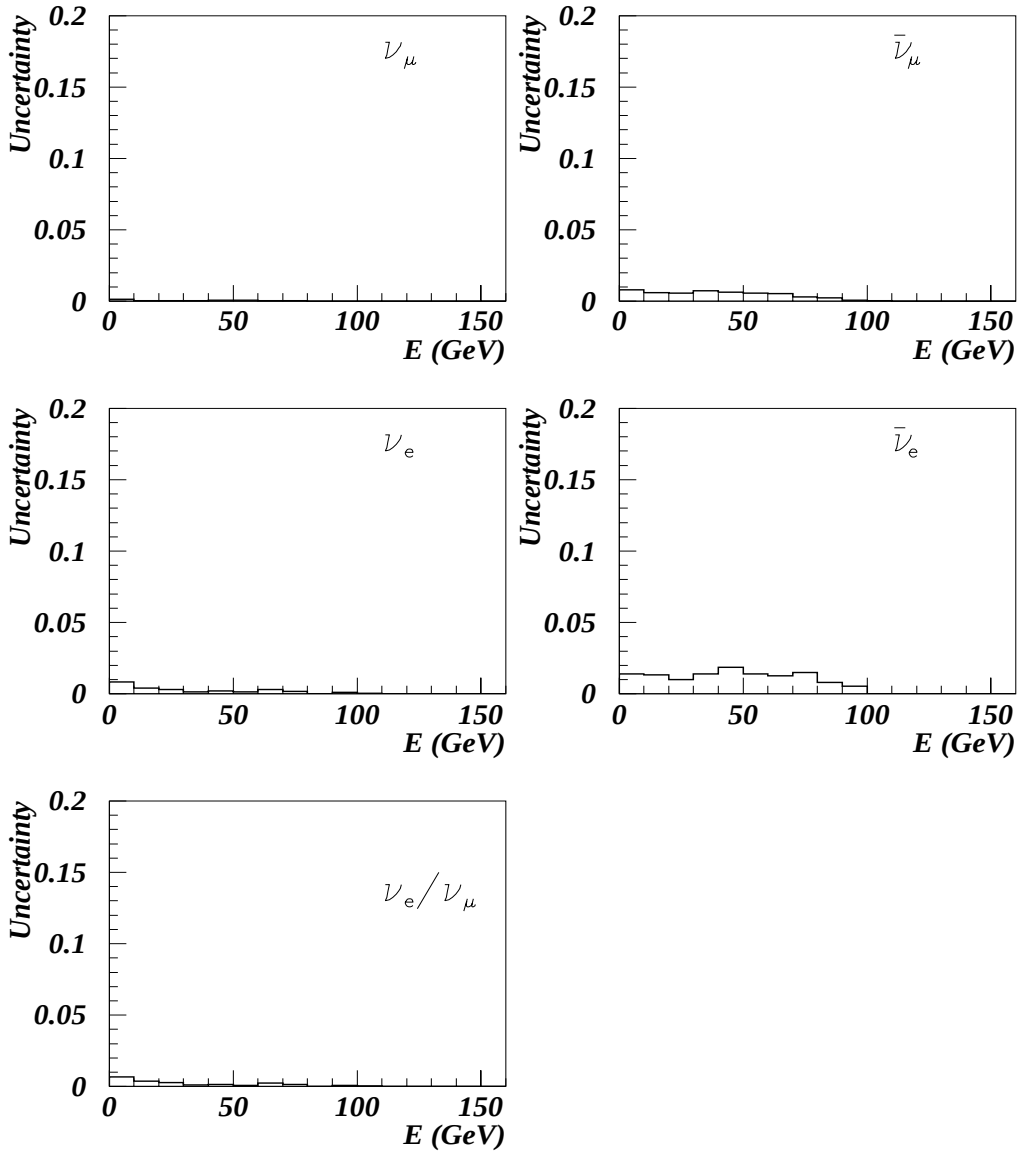


Figure 17: Energy dependent errors on neutrino fluxes and $\nu_e/\nu_\mu$ ratio from prompt neutrinos.

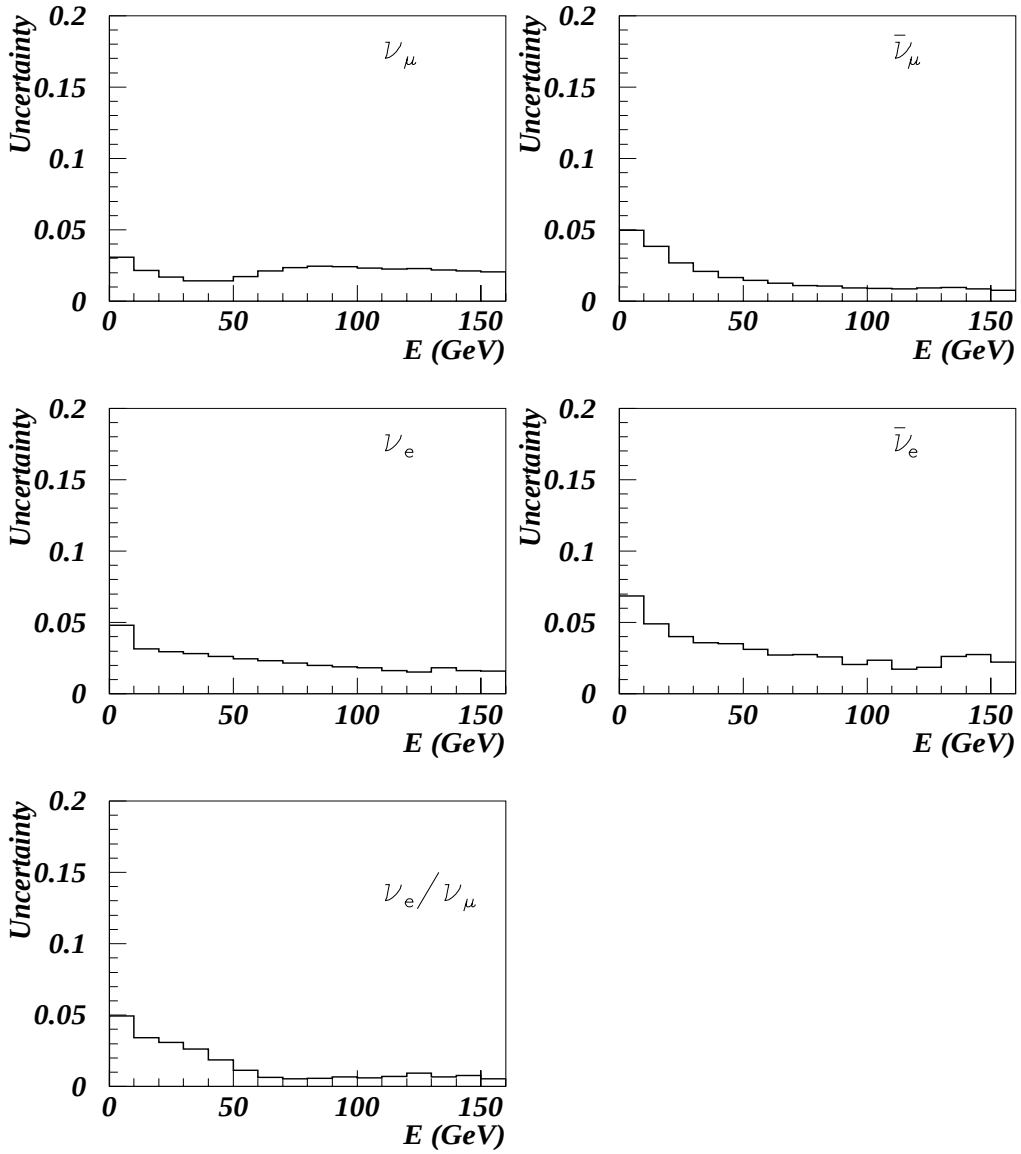


Figure 18: Energy dependent errors on neutrino fluxes and $\nu_e/\nu_\mu$ ratio from particle reinteractions.

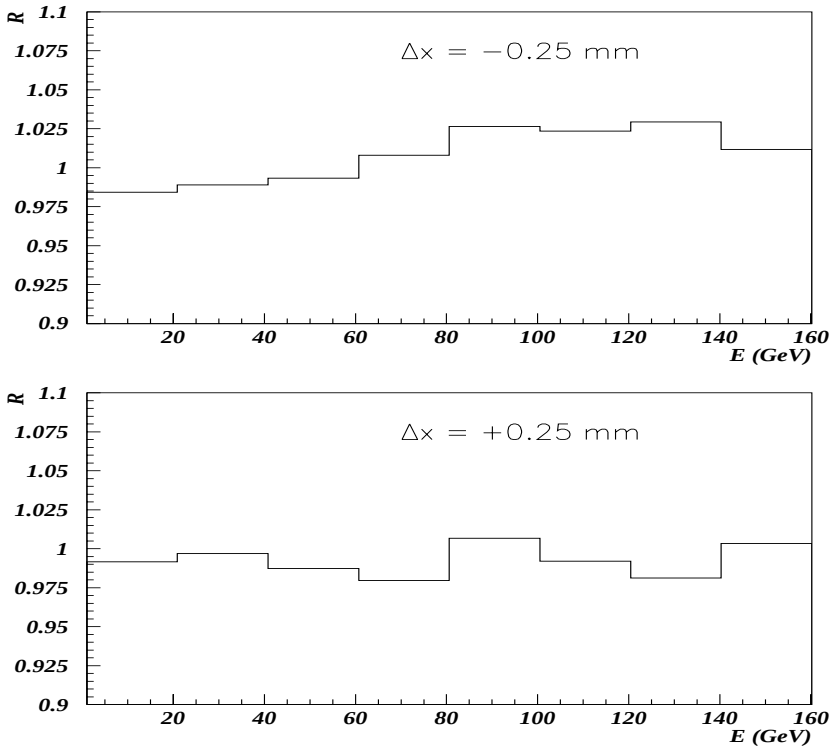


Figure 19: Energy dependent effects on $\nu_e/\nu_\mu$ ratio from $\Delta X = \pm 0.25$ mm proton-beam profile displacement.

deviation from unity of the reweighting function $f$ between 20 and 100 GeV/c and $D_{ave}$, the corresponding average deviation from unity, were determined from Fig. 7. $D_{max}$ was $10.0\%$, $15\%$, $17\%$, $27\%$ and $26.6\%$ for $\pi^+$, $K^+$, $\pi^-$, $K^-$ and $K^0_L$ respectively. The corresponding values for $D_{ave}$ were $5.8\%$, $4\%$, $15.3\%$, $26.5\%$ and $22.6\%$. The values $15.9\%$ and $10.0\%$ were assigned to "others".

Since the neutrinos produced by 450 GeV/c proton interactions downstream of the target affected the overall neutrino spectra similarly at all energies, the corresponding error was included wholly as a normalization error. Therefore the momentum spectrum of each meson type resulting from these proton interactions was modified by $D_{ave}$ for all momenta and the effect on the integral flux of each neutrino flavor was determined. Then the integral error on each neutrino flavor and on the $\nu_e/\nu_\mu$ ratio were determined by adding in quadrature the contributions from all the meson types.

The contributions of secondary reinteractions in the Be target and downstream of the target to the overall neutrino fluxes were found to be very energy dependent. Therefore the corresponding uncertainties were split into a normalization part, which was determined as for proton interactions downstream of the target, and an energy-dependent term. For the second term, the quantity $D_{shape} = \sqrt{D^2_{max} - D^2_{ave}}$ was determined for all the involved particles: $8.1\%$, $14.5\%$, $7.4\%$, $5.2\%$, $14.0\%$, and $11.2\%$ for $\pi^+$, $K^+$, $\pi^-$, $K^-$, $K^0_L$ and "others", respectively. The momentum spectrum of each meson type resulting from these

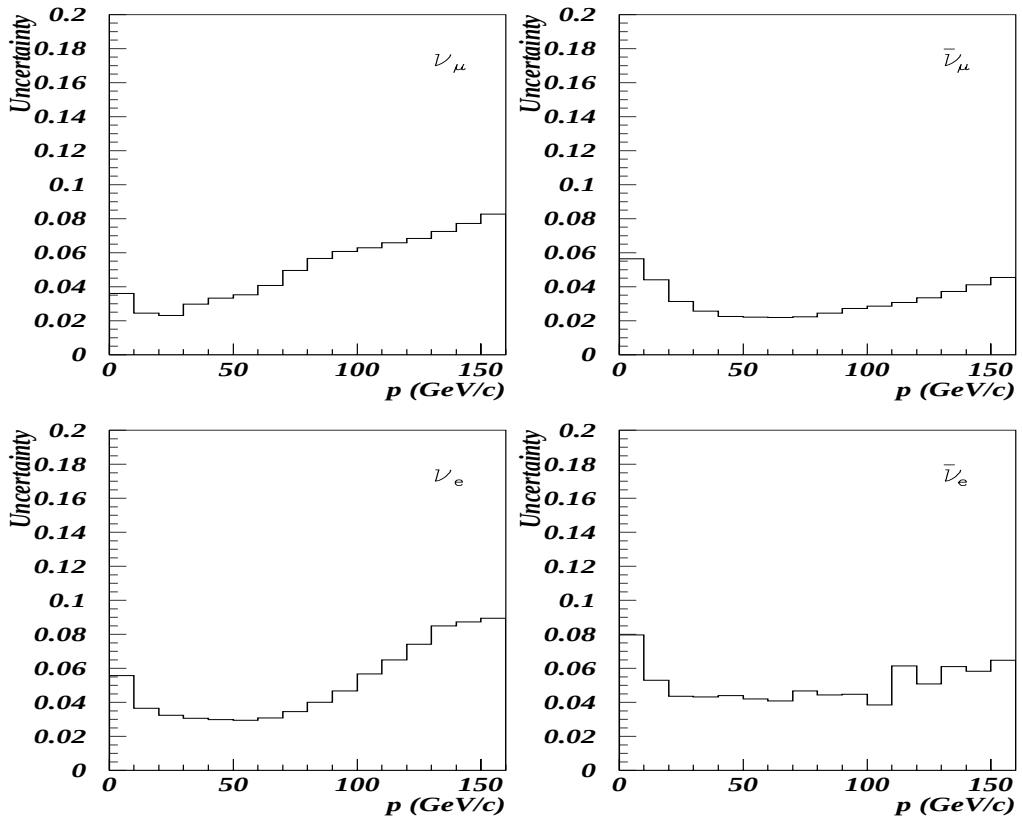


Figure 20: Total energy dependent error on the neutrino fluxes.

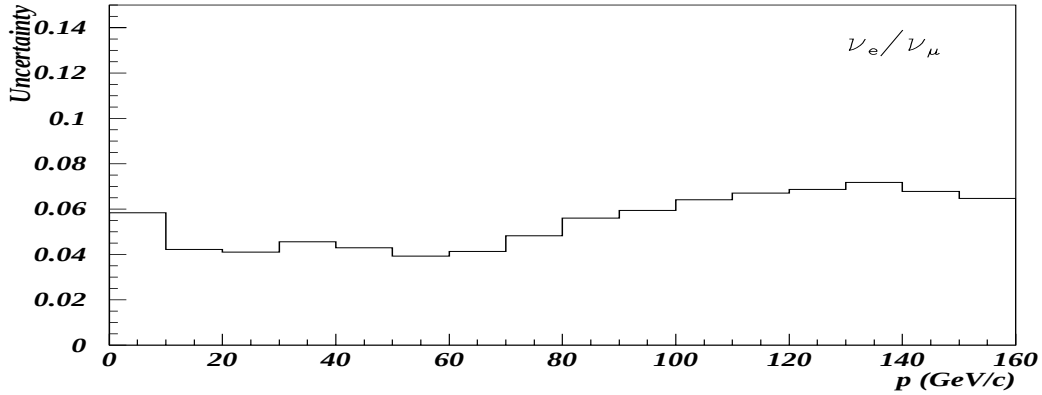


Figure 21: Total energy dependent error on the $\nu_e/\nu_\mu$ ratio.

reinteractions was modified by $D_{shape}$ for all momenta and the effect on the integral flux of each neutrino flavor was determined. Finally the energy dependent uncertainty on each neutrino flavor and on the $\nu_e/\nu_\mu$ ratio were determined by adding in quadrature all the contributions from the meson types.

| Source of uncertainty | $\nu_\mu$ | $\overline{\nu}_\mu$ | $\nu_e$ | $\overline{\nu}_e$ | $\nu_e/\nu_\mu$ |
|---|---|---|---|---|---|
| Yields of secondary particles | 0.034 | 0.029 | 0.039 | 0.064 | 0.036 |
| Proton int. downstr. of the target | 0.002 | 0.024 | 0.003 | 0.013 | 0.003 |
| Reinteractions of secondaries | 0.014 | 0.070 | 0.017 | 0.067 | 0.018 |
| Beam position and divergence | 0.056 | 0.021 | 0.058 | 0.035 | 0.002 |
| Collimators, horn and reflector | 0.007 | 0.034 | 0.015 | 0.024 | 0.011 |
| Amount of material | 0.012 | 0.022 | 0.007 | 0.012 | 0.005 |
| Total | 0.068 | 0.091 | 0.074 | 0.103 | 0.042 |

Table 6: Different contributions to normalization errors for neutrino fluxes.

### 4.3 Other sources of systematics

The uncertainty in the proton beam position relative to the target, was determined by the resolution of the mini-scan monitoring system used: $\sigma = 0.25$mm. The beam displacement $\Delta X = \pm 0.25$ mm in the horizontal plane produced, as expected, a variation of $5.6\%$ on $\nu_\mu$ and $5.8\%$ on $\nu_e$, and a little less for $\overline{\nu}_\mu$ and $\overline{\nu}_e$ that are mainly produced in the tertiary interactions. These values were included as normalization uncertainties (see tab. 6). It also resulted in an energy-dependent error of up to $2.3\%$ on the $\nu_e/\nu_\mu$ ratio (Fig. 19). A displacement of the proton beam by $\Delta Y = \pm 0.25$ mm in the vertical plane resulted in negligible effects on the neutrino fluxes. The effect of the uncertainty in the angular divergence of the primary proton beam on the neutrino fluxes was also found to be negligible.

The effect of the uncertainties in the current stability in the horn and reflector ($\pm 2\%$), the magnetic field inside their inner conductors, and of the alignment of collimators ($\pm 3$ mm), horn and reflector (upper limit 1 mm) were carefully studied [9]. Globally normalization errors which amount to $0.67\%$, $3.36\%$, $1.53\%$, $2.39\%$ and $1.11\%$ for $\nu_\mu$, $\overline{\nu}_\mu$, $\nu_e$, $\overline{\nu}_e$ and $\nu_e/\nu_\mu$ respectively were found.

Moreover the size of the possible inaccuracies in the simulation of the beam line elements was estimated by studying the differences between the measured and predicted spectra of $\overline{\nu}_\mu$ CC and $\overline{\nu}_e$ CC events, the most sensitive to secondary interactions in the beam-line. As a result the amount of material possibly missing in the simulation was

determined not to exceed the equivalent of a 1 cm thick aluminum slab placed downstream of the reflector, which produced a variation of $1.2\%$ for $\nu_\mu$ and $0.6\%$ for $\nu_e$ and only $0.5\%$ of $\nu_e/\nu_\mu$ ratio.

### 4.4 Summary of systematic uncertainties

All the systematic uncertainties described above, subdivided into energy-dependent and normalization (energy-independent) errors, were then combined in quadrature (see Figs. 20, 21 and Table 6). The resulting total normalization uncertainty was $6.8\%$, $9.1\%$, $7.4\%$ and $10.3\%$ for $\nu_\mu$, $\overline{\nu}_\mu$, $\nu_e$ and $\overline{\nu}_e$ respectively. Globally the fluxes of the four neutrino flavors at NOMAD were predicted with an overall uncertainty of about $8\%$ for $\nu_\mu$ and $\nu_e$, $10\%$ for $\overline{\nu}_\mu$, and $12\%$ for $\overline{\nu}_e$ (energy-dependent and normalization errors combined). The energy-dependent uncertainty achieved on the $\nu_e/\nu_\mu$ ratio ranged from 4 to $7\%$ whereas its normalization uncertainty was $4.2\%$.

## 5 Comparison with data and conclusions

Neutrino interactions in the NOMAD detector were generated via Monte Carlo according to the energy spectra and radial distributions as calculated for each neutrino species and the results were analyzed and compared to the data collected in NOMAD [4] with both polarities of the focusing devices and also with horn and reflector switched off [9]. Globally NOMAD studied more than 830000 charged current (CC) muon neutrino interactions in the positive focusing mode, $\sim 27000$ muon antineutrino CC-interactions in the negative focusing mode and $\sim 1600$ muon neutrino CC-interactions with horn and reflector off.

The neutrino energy was approximated by the "visible energy", defined as the sum of the energies of the charged lepton and of the hadrons observed in the final state. Since the $\nu_\mu \to \nu_e$ oscillations were looked for as an excess in the $\nu_e/\nu_\mu$ ratio, the Monte Carlo distribution of $\nu_\mu$ CC events was normalized, in the positive focusing, to the number of $\nu_\mu$ CC events in the data. The other Monte Carlo neutrino components were rescaled according to this $\nu_\mu$ CC normalization.

The comparison of the measured and the predicted neutrino energy spectra with positive focusing shows that the results of the simulations are in very good agreement with the data (Fig. 22). The shape of the $\nu_\mu$ CC energy spectrum is predicted to better than $2\%$ up to 150 GeV/c. The only statistically significant difference, of up to $8\%$ but smaller than the estimated systematic uncertainty, is observed in the $\overline{\nu}_\mu$ CC. Both the shape and the total number of $\overline{\nu}_e$ CC events are well reproduced, confirming the validity of the adopted $K^0_L$ description. Similar agreement was found in the negative focusing and horn/reflector

off samples [9], confirming the validity of the beam line simulation and allowing for the possibility to perform a sensitive search for the $\nu_\mu \rightarrow \nu_e$ oscillations at the WANF.

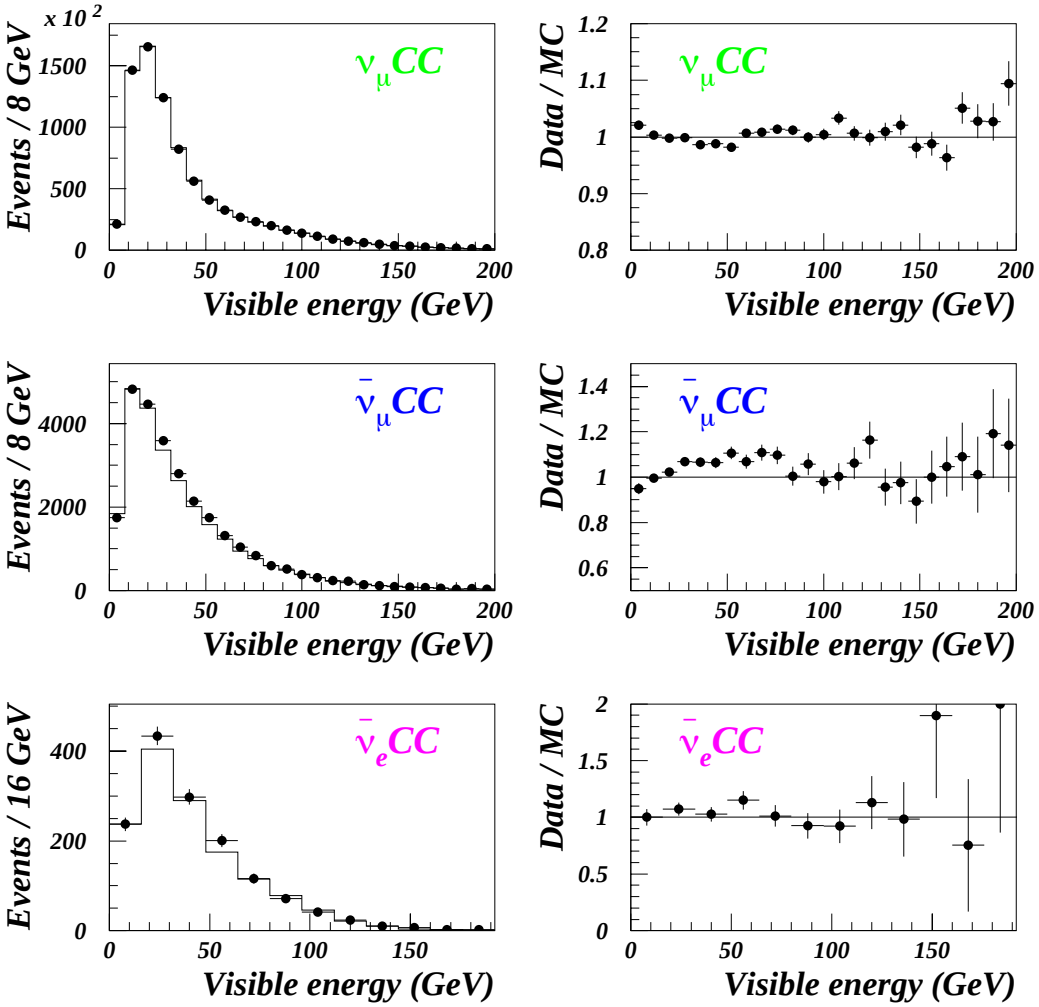


Figure 22: Left: neutrino energy spectra (left) for the data (points with error bars) and the Monte Carlo (histogram) for $\nu_m u$ CC, $\overline{\nu}_\mu$ CC and $\overline{\nu}_e$ CC interactions in neutrino mode and their corresponding ratios (right). Only the statistical errors are shown.

The corresponding $\nu_e$'s energy distributions for the data and the Monte Carlo as resulted in the $\nu_\mu \rightarrow \nu_e$ analysis are shown in Fig. 23 [15].

This WANF study was also relevant for the design and study of the expected performances of the new $\nu_\mu$ beam CNGS [16] from CERN SPS to Gran Sasso underground laboratory. In particular the normalization uncertainties of the $\nu_\mu$ and $\nu_e$ could be reduced significantly through a better knowledge of the beam position or a wider target in order

to minimize the number of protons missing it. Uncertainties as small as $\sim 4\%$ for $\nu_\mu$ flux and $\sim 3\%$ for the $\nu_e/\nu_\mu$ ratio can be predicted for the CNGS beam due to longer base-line, where the contribution of $K^0_L$ and of particle reinteractions are strongly reduced, and to the improved beam optics.

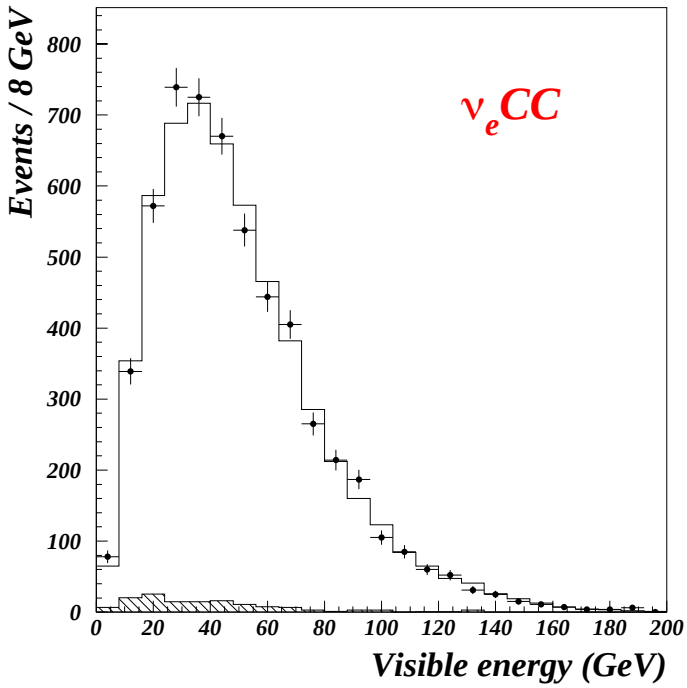


Figure 23: Neutrino energy spectra for the data (points with error bars) and the Monte Carlo (histogram) for $\nu_e$ CC. The Monte Carlo distribution is normalize using the predicted relative $\nu_e/\nu_\mu$. Only the statistical errors are shown. The background contribution is shown in the hatched histogram.

## 6 Acknowledgments

The contributions of A. Ferrari and P.R. Sala in the setting-up of the Monte Carlo code based on FLUKA package for the description of hadronic interactions and of V. Valuev for the particle transport studies, are gratefully acknowledged. Moreover we warmly thank L. Camilleri, P. Soler and V. Palladino for many interesting and stimulating discussions.

## References


[1] L. Casagrande et al., CERN Yellow report 96-06, 1996.

[2] NOMAD Collaboration, J. Altegoer et al., Nucl. Instr. and Meth. A 404 (1998) 96.

[3] CHORUS Collaboration, E. Eskut et al., Phys. Lett. B 497 (2001) 8, and references therein.

[4] NOMAD Collaboration, P. Astier et al., Nucl. Phys. N 611 (2001) 3.

[5] M.C. Gonzales-Garcia, J.J. Gomez-Cadenas, Phys. Rev. D 55 (1997), 1297;
B. Van de Vijver, P. Zucchelli, Nucl. Instr. and Meth. A 385 (1997) 91.

[6] A. Fasso' et al., in A. Kling, F. Barao, M. Nakagawa, L. Tavora, P. Vaz, eds., *Proceedings of the Monte Carlo 2000 Conference* (Springer-Verlag, Berlin, 2001) 955.

[7] H.W. Atherton et al., CERN Yellow Report 80-07, 1980.

[8] SPY Collaboration, G. Ambrosini et al., Eur. Phys. J. C 10 (1999) 605.

[9] NOMAD Collaboration, P. Astier et al., " Prediction of neutrino fluxes in the NOMAD experiment", CERN-EP/2003-032, hep-ex/0306022, to appear on Nucl. Instr. and Meth.

[10] R. Brun, F. Carminati, GEANT Detector Description and Simulation Tool, CERN Program Library Long Writeup W5013, 1993;
A. Fasso' et al., *Proceeding of the IV International Conference on Calorimetry in High Energy Physics*, La Biodola (Elba) 1993, Word Scientific (1994) 493.

[11] G. Collazuol and A. Guglielmi,"Monte Carlo Simulation of the Neutrino flux in NOMAD - I", NOMAD Memo 98-32, 1998, unpublished.

[12] G. Collazuol et al., Nucl. Instr. and Meth. A 449 (2000) 609.

[13] A. Ferrari and P.R. Sala, " The Physics of High Energy Reactions", in: A. Gandini, G. Reffo, eds., *Proceeding of Workshop on Nuclear Reaction Data and Nuclear Reactors Physics, Design and Safety* (World Scientific, Singapore, 1998) Vol. 2, 424.

[14] A.A. Borisov et al., Phys. Lett. B 369 (1996) 39, and M. Kirsanov, hep-ex/0106035.

[15] NOMAD Collaboration, P. Astier et al., " Search for $\nu_\mu \rightarrow \nu_e$ oscillations in the NOMAD experiment", CERN-EP/2003-038, hep-ex/0306037, to appear on Phys. Lett. B 570 (2003).

[16] G. Acquistapace et al., "The CERN neutrino beam to Gran Sasso", CERN 98-02, INFN/AE-98/05 (1998);
A.E. Ball et al., "CNGS: Update on secondary beam layout", SL-NOTE-2000-063 DI (CERN).